Cerebral Cortex, 2020;00: 1–19

doi: 10.1093/cercor/bhaa107
Original Article

ORIGINAL ARTICLE

Foxg1 Upregulation Enhances Neocortical Activity

Wendalina Tigani[1], Moira Pinzan Rossi[1,8], Osvaldo Artimagnella[1], Manuela Santo[1], Rossana Rauti[2,9], Teresa Sorbo[2], Francesco Paolo Severino Ulloa[3,10], Giovanni Provenzano[4], Manuela Allegra[5,11], Matteo Caleo[5,6], Laura Ballerini[2], Yuri Bozzi[5,7] and Antonello Mallamaci[1]

[1]Laboratory of Cerebral Cortex Development, Neuroscience Area, SISSA, Trieste 34136, Italy, [2]Laboratory of Neurons and Nanomaterials, Neuroscience Area, SISSA, Trieste 34136, Italy, [3]Laboratory of Bionanotechnologies, Neuroscience Area, SISSA, Trieste 34136, Italy, [4]Department of Cellular, Computational, and Integrative Biology (CIBIO), University of Trento, Trento 38123, Italy, [5]Neuroscience Institute, Neurophysiology Section, National Research Council (CNR), Pisa 56124, Italy, [6]Department of Biomedical Sciences, University of Padua, Padua 35121, Italy, [7]Center for Mind/Brain Sciences, University of Trento, Trento 38068, Italy, [8]Current address: AgenTus Therapeutics, Inc., Cambridge CB4 OWG, United Kingdom, [9]Current address: Dept. Biomedical Engineering, Tel Aviv University, Tel Aviv 6997801, Israel, [10]Current address: Cell Biology Dept, Duke University Medical Center, Duke University, Durham NC-27710, USA and [11]Current address: Laboratory G5 Circuits Neuronaux, Institut Pasteur, Paris 75015, France

Address correspondence to Antonello Mallamaci, Lab of Cerebral Cortex Development, SISSA, via Bonomea 265, Trieste 34136, Italy.
Email: amallama@sissa.it
[†]Wendalina Tigani, Moira Pinzan Rossi, Osvaldo Artimagnella and Manuela Santo have contributed equally to this work

Abstract

Foxg1 is an ancient transcription factor gene orchestrating a number of neurodevelopmental processes taking place in the rostral brain. In this study, we investigated its impact on neocortical activity. We found that mice overexpressing *Foxg1* in neocortical pyramidal cells displayed an electroencephalography (EEG) with increased spike frequency and were more prone to kainic acid (KA)-induced seizures. Consistently, primary cultures of neocortical neurons gain-of-function for *Foxg1* were hyperactive and hypersynchronized. That reflected an unbalanced expression of key genes encoding for ion channels, gamma aminobutyric acid and glutamate receptors, and was likely exacerbated by a pronounced interneuron depletion. We also detected a transient *Foxg1* upregulation ignited in turn by neuronal activity and mediated by immediate early genes. Based on this, we propose that even small changes of *Foxg1* levels may result in a profound impact on pyramidal cell activity, an issue relevant to neuronal physiology and neurological aberrancies associated to *FOXG1* copy number variations.

Key words: *Foxg1*, immediate early genes, neuron hyperactivity, West syndrome

Introduction

Foxg1 is a pleiotropic effector mastering a variety of neurodevelopmental subroutines occurring within the rostral brain. It specifies the telencephalic field (Hanashima et al. 2007), promotes subpallial programs (Manuel et al. 2010), and activates paleo- and neocortical morphogenesis (Muzio and Mallamaci 2005). Besides, *Foxg1* stimulates neural precursor self-renewal (Martynoga et al. 2005) and orchestrates temporal articulation of neocorticogenesis. Stable *Foxg1* silencing paves the way to Cajal–Retzius cell generation (Hanashima et al. 2004). A short-term decline of it followed by reactivation is instrumental to birth, radial migration, proper laminar commitment, and architectural

maturation of later born pyramidal neurons (Martynoga et al. 2005; Miyoshi and Fishell 2012; Toma et al. 2014; Chiola et al. 2019). *FOXG1* upregulation occurring in autism spectrum disorder (ASD) patient-specific neuro-organoids has been reported to underlie an increase of neocortical interneurons, due to aberrant hyperproliferation of their progenitors (Mariani et al. 2015). On the other side, ablation of one *Foxg1* allele decreases the number of these cells, due to their defective migration from basal forebrain (Shen et al. 2019). Moreover, a reduction of *Foxg1* levels also perturbs interneuronal maturation. It evokes neurite hypertrophy (Shen et al. 2019), deregulates *Gad2* (Patriarchi et al. 2016), and reduces their electrical activity (Zhu et al. 2019). In this respect, a dampened interneuronal function has been suggested to contribute to seizures occurring in patients with structural *FOXG1* mutations (Mitter et al. 2018; Vegas et al. 2018). Next, a reduction of *Foxg1* levels in neopallial stem cells is required for their progression to glial lineages (Brancaccio et al. 2010; Falcone et al. 2019). Finally, as suggested by the devastating Rett-like and West syndromes affecting patients with defective or supranumerary *FOXG1* alleles, respectively (Florian et al. 2011; Striano et al. 2011), fine-tuning of *FOXG1* expression levels is globally crucial to proper brain morphogenesis and function.

We speculated that, in addition to its impact on dendritogenesis and laminar identity, persistent expression of *Foxg1* in pyramidal neurons might further modulate their functional regime. We tested this hypothesis in vivo and in vitro. We found that *Foxg1* upregulation in neocortical pyramids increased their electrical activity and made *Foxg1*-GOF mice more prone to kainic acid (KA)-induced seizures. Unbalanced expression of key genes implicated in GABAergic and glutamatergic transmission likely underlie these phenomena, possibly exacerbated by a concomitant reduction of interneurons and astrocytes. We also found that, in turn, a transient *Foxg1* upregulation was triggered by electrical activity. The resulting positive feedback loop between *Foxg1* expression and electrical activity may make pyramidal neurons sensitive to even small changes of *Foxg1* expression products. That may be relevant to normal control of neocortical functional regime and account for neurological aberrancies stemming from *FOXG1* copy number variations (Florian et al. 2011; Seltzer et al. 2014).

Materials and Methods

This section includes generation of lentiviral vectors, mouse handling, generation and selection of transgenic mouse lines, histology, brain section immunofluorescence, EEG recordings, behavioral observation of KA-induced seizures, in situ hybridization, corticocerebral cultures, Arc-SARE evaluation of neuronal activity, calcium imaging, cell culture immunofluorescence, photography and image processing, RNASeq, quantitative RT-PCR, western blot analysis, image acquisition, and statistical evaluation of results. For each of them, full details are provided in Supplementary Information.

Results

Generation of Transgenic Mice Overexpressing *Foxg1* in Deep-Layer Neocortical Projection Neurons

To investigate etiopathogenic mechanisms linking exaggerated *FOXG1* allele dosage to pronounced neuronal hyperactivity peculiar to West syndrome patients, we generated mice gain of function for *Foxg1*, by zygotic lentiviral transgenesis and TetON/OFF technology (Supplementary Fig. 1A). Three single transgene insertion, CD1-congenic male founders were obtained. They were scored for transgene expression, in vitro and in vivo. Two of them performed very poorly and were discarded, and the third one (founder "E") was selected and employed for this study.

We investigated the *Tre-Foxg1-IRES-Egfp* spatiotemporal expression pattern in *Foxg1*$^{tTA/+}$; *Tg:Tre-Foxg1-IRES-Egfp*$^{+/-}$ compound mutants (Hanashima et al. 2002), and we compared it with the distribution of the *Foxg1* protein, normally detectable throughout telencephalon since E9.5. We found that the transgene was activated at E14.5, when a weak Egfp signal, restricted to the neocortical field, could be found (Supplementary Figs 2A and 3A). A stronger signal, again limited to neocortex, was detectable at E16.5 (Fig. 1A,B and Supplementary Fig. 2B). This pattern remained substantially unchanged at later developmental ages (Fig. 1C and Supplementary Fig. 2C), until P7 (Fig. 1D,F and Supplementary Fig. 2D) and beyond (not shown). Within neocortex, transgene products showed a dynamic radial distribution. At E14.5, a faint signal was detectable in a few cells located in the uppermost cortical plate (Supplementary Fig. 3A, arrowheads). At E16.5, a large fraction of cortical plate cells were intensely immunoreactive for Egfp, which also stained large bundles of presumptive corticofugal fibers running within the subplate and below it (Fig. 1B and Supplementary Fig. 3B). A similar pattern was retained at P0 and P7, when—however—the cortical plate signal was prevalently limited to deeper layers (Supplementary Fig. 3C, upper row, and *D*) and the Egfp-positive fibers were clustered just above the subventricular zone (Supplementary Fig. 3C, upper row, and *D*, arrows) and further detectable while crossing the striatal field (Supplementary Fig. 3C, lower row, arrows). Remarkably, at none of the developmental ages analyzed, transgene activity was detectable within periventricular proliferative layers, where the endogenous *Foxg1* was conversely active, albeit at low levels (Fig. 1B and Supplementary Fig. 3A–C, asterisks).

Next, we addressed the identity of neural cells expressing the transgene. We found that almost the totality of them was postmitotic neurons co-expressing Egfp and two established pan-neuronal markers, Tubb3 and NeuN, at E16.5 through P7 (Fig. 1C,D and Supplementary Fig. 4). Based on obvious morphological criteria (a thin apical dendrite emerging from a radially oriented soma (Fig. 1C and Supplementary Fig. 4, arrows)), these cells turned out to be pyramidal neurons. Comparison of their P7 radial distribution with DAPI staining as well as with the profiles of three established layer-specific markers, FoxP2 (layer VI), Ctip2 (layer V), and Cux1 (layers IV–II) (Molyneaux et al. 2007), suggested a presumptive layer VI/V identity (Supplementary Fig. 6). To corroborate specific *glutamatergic* identity of these cells, we coimmunoprofiled P7 and P15 brains for Egfp and three GABAergic interneurons' markers, parvalbumin (PV), somatostatin (SST), and calretinin (CR) (Wamsley and Fishell 2017). As expected, no Egfp colocalization with such markers was detected at all (Fig. 1E). Finally, we coimmunoprofiled transgenic P7 brains for Egfp and the astrocyte marker S100β (Raponi et al. 2007). Again, no colocalization was observed, confirming that transgene-expressing cells were deep-layer projection neurons (Fig. 1F).

Neural Hyperactivity–Hyperexcitability of *Foxg1*-GOF Mice

To preliminarily assess the impact of *Foxg1* overexpression on neocortical projection neurons activity, primary cultures of neocortical precursors, originating from E16.5 *Foxg1*-GOF

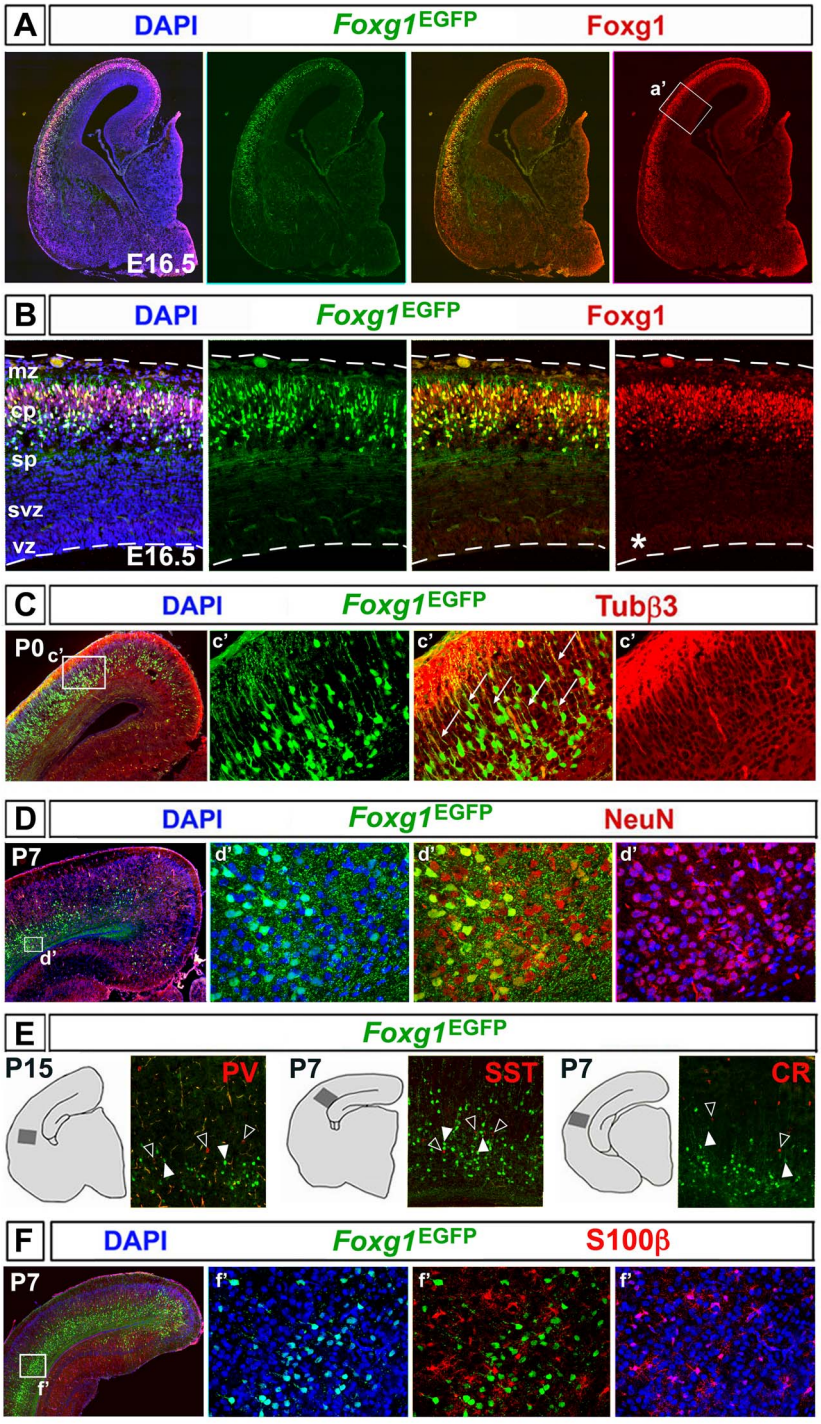

Figure 1. Expression pattern of the *Foxg1-promoter*-tTA-driven, *Foxg1-IRES-EGFP* transgene. (*A* and *B*) Restriction of transgene products to the cortical plate of the E16.5 neocortical primordium. In (*B*), a high power magnification of the a′ boxed region of (*A*) is shown. The asterisk highlights the vz *Foxg1* expression domain. (*C* and *D*) Confinement of transgene products to Tubb3$^+$ and NeuN$^+$ pyramidal neurons within deep layers of neonatal gray matter. In both rows, high-power magnifications in columns 2–4 correspond to boxed insets in column 1 (c′ and d′, respectively). Arrows in (*C*, 3rd panel) point to Tubb3$^+$ apical dendrites, connecting neuronal somata to the marginal edge of the cortical wall. (*E* and *F*) Absence of transgene products in neocortical parvalbumin$^+$ (PV$^+$), somatostatin$^+$ (SST$^+$), and calretinin$^+$ (CR$^+$) interneurons as well as in neocortical S100β^+ astrocytes. In (*E*), high-power pictures refer to dark gray areas within the associated silhouettes, and solid and empty arrowheads point to EGFP$^+$ and interneuron marker$^+$ cells, respectively. In (*F*), high-power magnifications in columns 2–4 correspond to the boxed region in column 1 (f′). Abbreviations: mz, marginal zone; cp, cortical plate; sp, subplate; svz, subventricular zone; vz, ventricular zone; *Foxg1*^{EGFP}, *TREt-Foxg1-IRES-EGFP* transgene-driven EGFP.

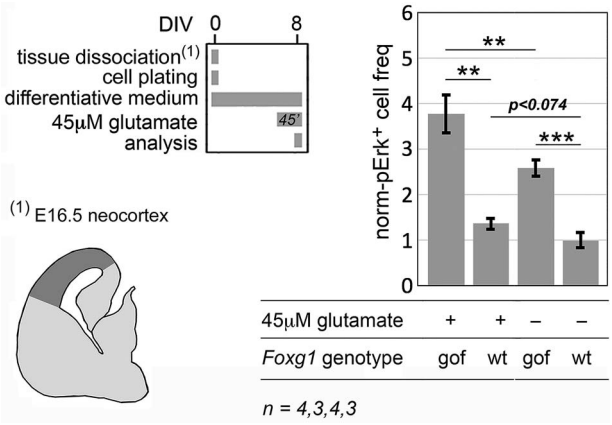

Figure 2. Nuclear-pErk1^{+} immunoprofiling of E16.5 + DIV8, *Foxg1*-GOF (*Foxg1*$^{tTA/+}$;*Tg:TREt-Foxg1-cds-IRES-EGFP*$^{+/-}$) and *wt* (*Foxg1*$^{+/+}$;*Tg:TREt-Foxg1-cds-IRES-EGFP*$^{-/-}$) neocortical precursors, terminally (45 min) pulsed by 45 μM glutamate. Protocol and results are shown. Data normalized against *wt*-not pulsed samples. Absolute nuclear-pErk1^{+} cell frequency in *wt*/not-pulsed samples = 0.10 (see Supplementary Materials and Methods: Immunofluorescence). Results evaluated by *t*-test (unpaired, one-tailed). *n*, number of biological replicates (i.e., independently transduced samples, each including >1200 cells); $^{**}P < 0.01$; $^{***}P < 0.001$.

(*Foxg1*$^{tTA/+}$;*Tg:Tre-Foxg1-IRES-Egfp*$^{+/-}$) embryos and their littermate wt controls, were immunoprofiled at DIV8 for the activity reporter pErk1 (Tyssowski et al. 2018), in baseline conditions as well as upon terminal stimulation by 45 μM glutamate. Normalized against wt-unstimulated samples, the prevalence of pErk1^{+} cells equaled 1.37 ± 0.11, 2.59 ± 0.18 and 3.78 ± 0.42 in wt-stimulated, *Foxg1*-GOF-unstimulated, and *Foxg1*-GOF-stimulated samples, suggesting that *Foxg1* overexpression promoted the activity of neocortical cultures both in baseline conditions ($p_{Foxg1\text{-GOF/unstim-vs-wt/unstim}} < 0.001$) and upon acute stimulation ($p_{Foxg1\text{-GOF/stim-vs-wt/stim}} < 0.003$) (Fig. 2 and Supplementary Fig. 5).

Next, to investigate consequences of *Foxg1* overexpression in vivo, P41 *Foxg1*-GOF (*Foxg1*$^{tTA/+}$;*Tg:Tre-Foxg1-IRES-Egfp*$^{+/-}$) mice and wt controls, awake and freely moving, were profiled by EEG. Electrical activity was monitored within the hippocampus. Albeit not expressing the transgene, in fact, this structure receives extensive neocortical inputs via entorhinal cortex and reverberates them, so acting as a comfortable proxy of global neocortical activity. A bipolar electrode was placed between Cornu Ammonis field 1 (CA1) and dentate gyrus (DG)/hilus regions (Fig. 3A). It was secured to the skull and electrical activity was monitored for 3 days, 2 h per day. The EEG was inspected paying special attention to frequency and temporal distribution of spikes (Fig. 3B). Interestingly, both total spike frequency and interictal cluster frequency were increased by about 50% in *Foxg1*-GOF mutants as compared to controls (with $n = 4,4$, and $P < 0.01$ and $P < 0.02$, respectively). Ictal cluster frequency was increased by >3 times; however, this did not reach statistical significance. Isolated spike frequency was unaffected (Fig. 3C). Altogether, these data point to an appreciable increase of coordinated neuronal activity occurring in *Foxg1*-GOF mutants compared to controls.

Then, to corroborate these findings, we challenged *Foxg1*-GOF mutants with the proconvulsant glutamatergic agonist KA, employing *Foxg1*-loss of function (*Foxg1*-LOF) (Hanashima et al. 2002) and "wild-type" mice as controls. We administered P35 animals with 20 mg/kg KA, by intraperitoneal injection, and monitored their behavior over the following 2 h. Every 10 min, a score was given, according to Racine's staging criteria (Racine 1972) (Fig. 4A). The majority of animals did not go above Racine stage (RS) 3 (repetitive movements and head bobbing; 5/14, 12/17, and 7/9, as for GOF, WT, and LOF, respectively), a subset of them reached RS4 (limbic motor seizure; 4/14, 4/17, and 2/9, as for GOF, WT, and LOF, respectively). Only a few got up to RS5, continuous rearing and falling, and more (5/14, 1/17, and 0/9 in case of GOF, WT, and LOF, respectively) ($P < 0.073$, χ-square test) (Fig. 4B). Longitudinal analysis of data showed that, for each genotype, RS increased progressively from the onset of the experiment to about 1 h later, then smoothly declining. The RS(*t*) curve of the GOF group was on average 1.3 units above WT controls (the corresponding GOF/WT gap was only 0.3). In particular, the distance between the GOF and the WT curves peaked at 90 and 100 min, reaching 1.7 and 1.9, respectively, with $P < 0.01$ (ANOVA) in both cases (Fig. 4C). Altogether, these data point to a remarkable increase of neuronal excitability, occurring in GOF models compared to controls, and rule out that such effect may stem from dominant negative effects.

Finally, upon completion of Racine tests, mice were sacrificed and their brains snap-frozen for subsequent analysis. Brains were sliced and profiled by non-radioactive in situ hybridization, for expression of the *c-fos* immediate early gene. Within *Foxg1*-GOF brains, *c-fos*-mRNA was strongly activated throughout the hippocampus, including the DG, as well as in a large number of scattered neocortical cells. As for *wt* brains, the *c-fos* signal was robust in CA3, less pronounced in CA1 and DG, limited to a few cells within neocortex. Finally, *c-fos* activation was generally weaker in *Foxg1*-LOF brains (Fig. 4D). This scenario is consistent with behavioral data reported above and strengthens the hypothesis that a specific increase of neuronal activity occurred in neocortex of *Foxg1*-GOF mutants.

Histogenetic Aberrancies of *Foxg1*-GOF Mice

We hypothesized that the neurological profile of our mutants might first reflect gross histogenetic aberrancies, triggered by *Foxg1* overexpression in neocortical projection neurons.

To test this hypothesis, we first scored *Foxg1*-GOF, P0 and P7 neocortices for their lamination pattern. At P0 (Fig. 5A), the layer VI marker FoxP2 was slightly downregulated, the layer V marker Ctip2 spread into deeper gray matter, and Cux1 (normally expressed by layers IV–II) was dramatically downregulated. A consistent scenario was detectable at P7 (Supplementary Fig. 6). Closely packaged in VI layer of WT neocortex, FoxP2^{+} cells were loosely distributed through layers VI and V of GOF mutants. Ctip2^{+} cells partially spread into layer VI (arrows). Cux1^{+} layer IV–II was halved in its radial extension. The altered expression of these cortical markers points to perturbed differentiation/segregation of layer V and layer VI neurons as well as to an inhibition of layer IV–II programs in *Foxg1*-GOF mutants, consistent with Hou et al. (2019).

Next, we inspected the neocortex of P35 GOF mutants for spatial frequency of GABAergic interneurons, expressing PV, SST, and CR. We detected a generalized reduction of PV^{+} cells ($-42.57 \pm 3.27\%$, $P < 0.0005$, $n = 3,6$), particularly pronounced throughout layers VI–II and rostral neocortex. It did not reflect a dominant negative effect, as *Foxg1*-LOF mutants did not replicate it (Fig. 5B and Supplementary Table 1). SST^{+} and CR^{+} interneurons were mainly unaffected, except a local decline of the former in white matter ($-31.09 \pm 5.50\%$, $P < 0.020$, $n = 3,3$)

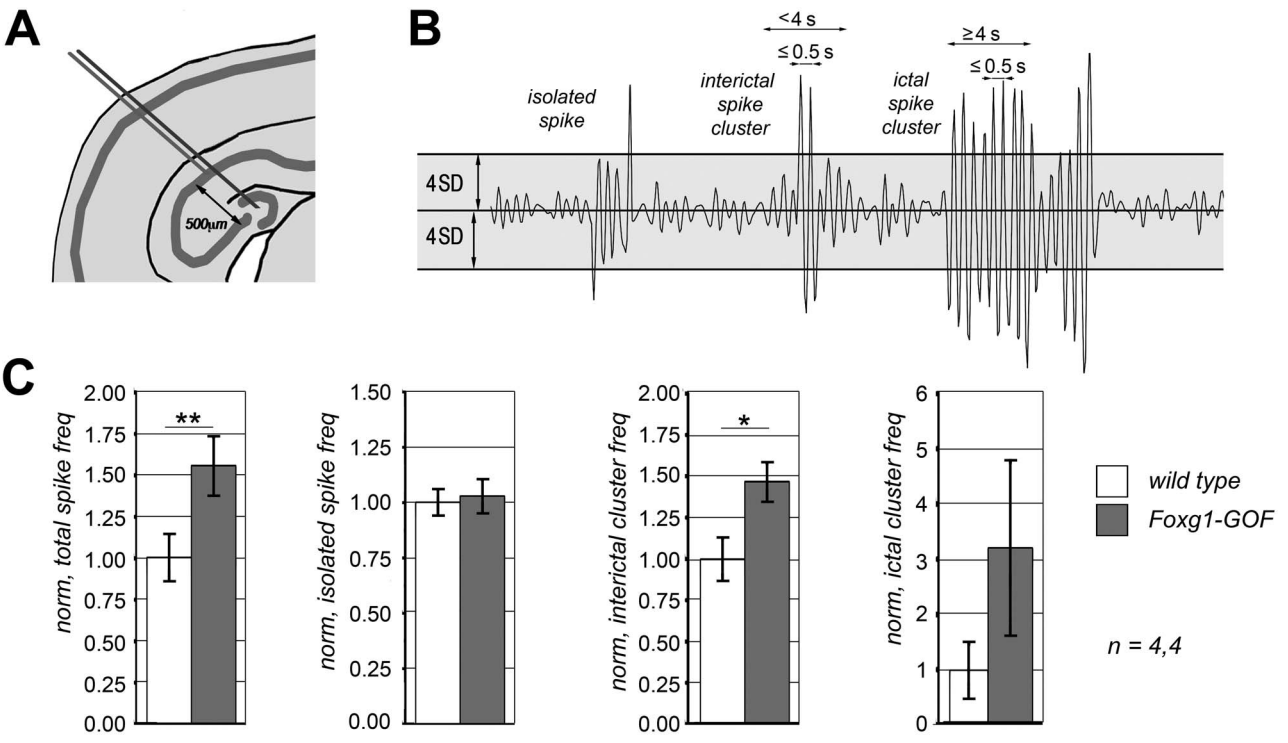

Figure 3. EEG recordings of P41 *Foxg1*-GOF (*Foxg1*$^{tTA/+}$;*Tg:Tre-Foxg1-IRES-Egfp*$^{+/-}$) and *wt* (*Foxg1*$^{+/+}$;*Tg:TREt-Foxg1-IRES-Egfp*$^{-/-}$) mice. (*A*) Schematics of bipolar electrodes placement into the hippocampal field. (*B*) Definition of spikes (as voltage fluctuations exceeding 4 standard deviations); classification of spikes (as isolated or clustered, if 1 or ≥2 within 0.5 s, respectively); and spike clusters (as interictal and ictal, if lasting <4 s and ≥4 s, respectively). (*C*) Graphical summary of control-normalized (1) total spike frequency, (2) isolated spike frequency, (3) interictal spike cluster frequency, and (4) ictal spike cluster frequency, in *Foxg1*-GOF and control mice. Absolute, control average values were 500, 150, 95, and 0.25 events/10 min, respectively. Electrical activity monitored over 3 days, 2 h per day, in awake conditions. *n*, number of biological replicates (i.e., individual mice); *$P < 0.05$; **$P < 0.01$.

and of the latter in medial neocortex (−61.25 ± 14.42%, $P < 0.009$, $n = 3,3$) (Supplementary Fig. 7 and Supplementary Table 1).

Finally, we scored *Foxg1*-GOF cortices for S100β^+ astrocytes. At P0, the neocortical spatial frequency of these cells was reduced by 21.0 ± 3.6% compared to *wt* controls ($P < 0.05$). At the same age, *Foxg1*-LOF mutants showed an opposite trend (+28.6 ± 9.3%, compared to *wt*), and the difference between *Foxg1*-GOF and -LOF brains was statistically significant ($P < 0.03$) (Fig. 5C and Supplementary Table 2). At P7, *Foxg1*-GOF mutants still showed a reduction of S100β^+ astrocytes (−15.6 ± 2.4%, $P < 0.07$, $n = 3,6$), specifically pronounced in lateral neocortex (−15.9 ± 4.1%, $P < 0.03$) as well as in layers I and II–IV (−26.4 ± 2.6%, $P < 0.05$, and −19.6 ± 4.9%, $P < 0.05$, respectively). As suggested by the different distribution of S100β^+ cells in *Foxg1*-LOF neocortices, this phenomenon hardly reflected a dominant-negative (DN) effect (Fig. 5D and Supplementary Table 2). Intriguingly, *Fgf9*, a key promoter of astroblast proliferation (Seuntjens et al. 2009), was robustly downregulated in *Foxg1*-GOF mice (Supplementary Fig. 8), suggesting that the decreased astroglial density peculiar to these mutants might originate from a non-cell autonomous, neocortical astrogenic deficit.

Hyperactivity of *Foxg1*-GOF Neocortical Cultures

To corroborate the hypothesis that *Foxg1* overexpression increases neocortical activity and preliminarily assess the possibility to dissect such phenomenon in cultures of *wt* neocortical precursors engineered by dedicated lentiviral effectors, we generated *Foxg1*-GOF preparations via somatic lentiviral transgenesis and probed them by a genetically encoded, delayed activity reporter (Kawashima et al. 2009). Specifically, DIV7 cultures originating from E16.5 neocortical precursors, harboring 1) a Tet^{ON}-controlled *Foxg1* transgene, 2) a d2EGFP reporter under the control of the "*Arc*-SARE-enhancer/minimal promoter (ArcSAREp)" neuronal activity-responsive element, and 3) a constitutively expressed *PGKp-RFP* normalizer, were employed. Upon pre-terminal TTX silencing, they were stimulated by Bdnf and finally profiled by cytofluorometry (Fig. 6A). Signal specificity was assessed by dedicated, Bdnf^{OFF} controls (not shown). Interestingly, the median d2EGFP/RFP fluorescence ratio, providing a cumulative index of neuronal activity over the previous 6 h, was upregulated by 1.60 ± 0.10 folds in *Foxg1*-GOF samples compared to controls ($P < 0.003$) (Fig. 6B), suggesting that *Foxg1* overexpression promoted neuronal activity.

To strengthen these findings and get insight into cellular mechanisms underlying them, we reinvestigated the impact of *Foxg1* on basal activity of neocortical cultures by fluorescence calcium imaging (Bosi et al. 2015; Rauti et al. 2016). Here, *Foxg1* was dampened by RNAi or, alternatively, upregulated by TetON transgenesis. In the latter case, transgene overexpression was pan-neural (sustained by the *Pgk1* promoter), specifically restricted to astrocytes or neurons (driven by *Gfap*- and *Syn*-promoters, respectively) or further confined to glutamatergic neurons (by means of the *CaMKII*-promoter) (Fig. 7A). Fluorescence fluctuations were recorded and analyzed by dedicated softwares. Three indices, representative of network activity, were calculated: 1) prevalence of spontaneously active

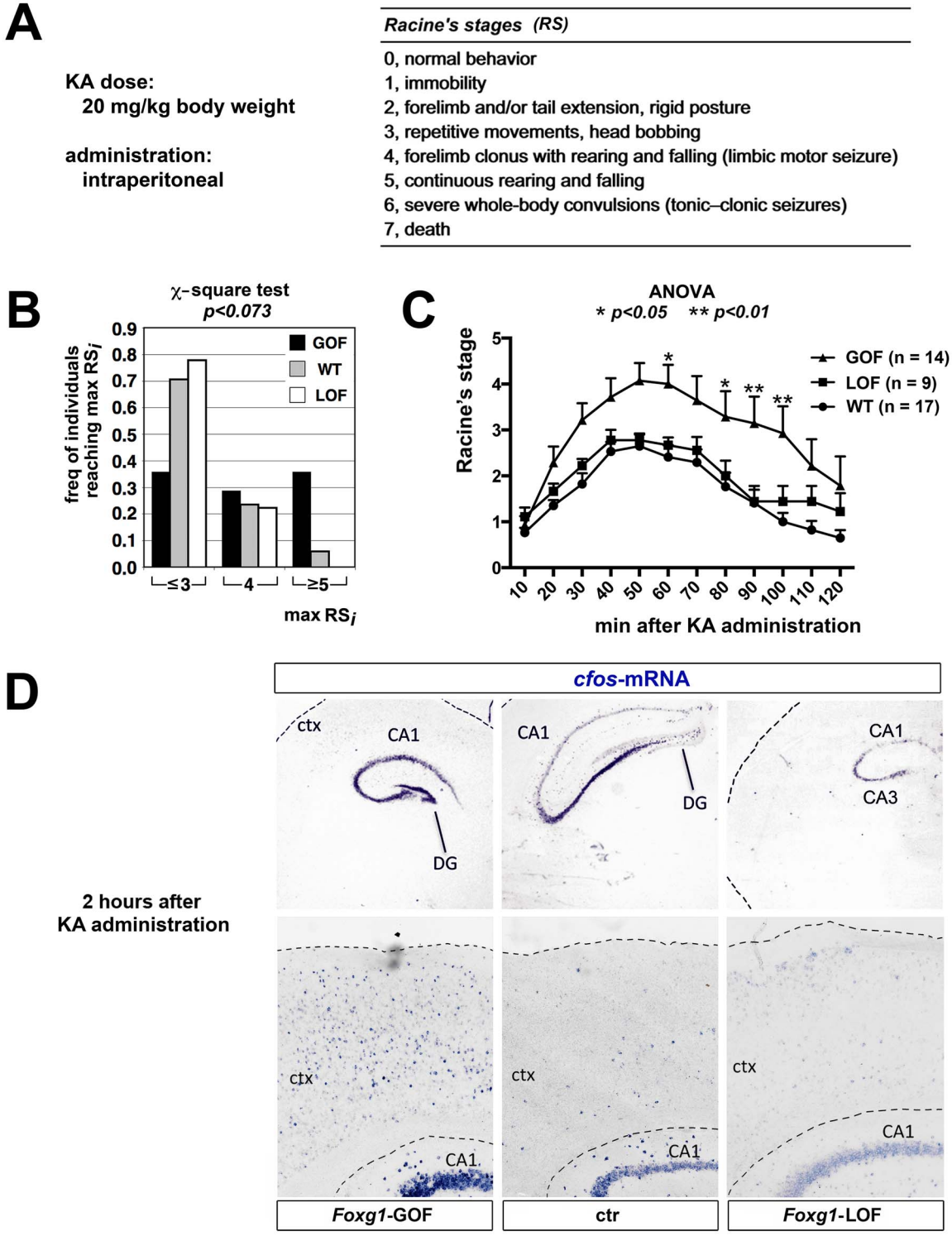

Figure 4. Comparative behavioral–molecular profiling of *Foxg1*-GOF, *Foxg1*-LOF, and wt, P35 mice upon proconvulsant stimulation. (*A*) Details of proconvulsant mice stimulation and subsequent Racine Staging (RS). (*B*) Distribution of individuals of distinct genotypes in groups reaching different maximal RS values and (*C*) temporal RS (average ± SEM) progression in individuals of different genotypes. Statistical significance of results assessed by χ-square (*B*) and ANOVA (*C*) assays, respectively. $^{*}P < 0.05$; $^{**}P < 0.01$. (*D*) Acute *c-fos* in situ hybridization of KA-treated mice, upon completion of Racine profiling, mid-frontal brain sections. Throughout Figure 3, "*Foxg1*-GOF" refers to *Foxg1*$^{tTA/+}$;*TREt-Foxg1-IRES-Egfp*$^{+/-}$ mutants; "*wt*" refers to data from pooled *Foxg1*$^{+/+}$;*TREt-Foxg1-IRES-Egfp*$^{-/-}$ and *Foxg1*$^{+/+}$;*TREt-Foxg1-IRES-Egfp*$^{+/-}$ animals, among which no statistically significant differences were previously found; and "*Foxg1*-LOF" to *Foxg1*$^{tTA/+}$;*TREt-Foxg1-IRES-Egfp*$^{-/-}$ mutants. Abbreviations: maxRS$_i$, Racine stage, maximal animal-specific value; ctx, cortex; CA1–3, Cornu Ammonis 1–3 fields.

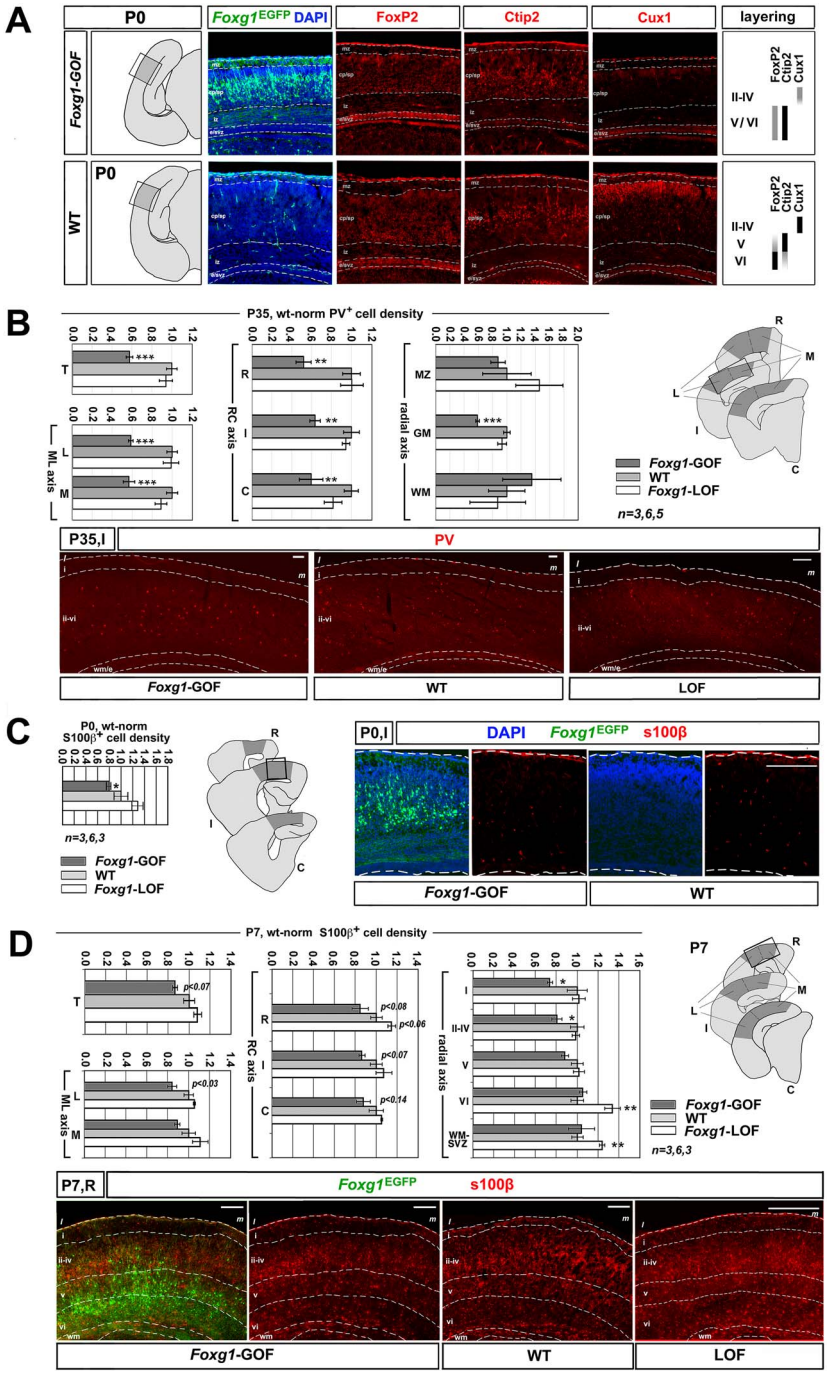

Figure 5. Histogenetic anomalies of *Foxg1*-GOF mutants. (*A*) P0 neocortical layering. Shown are neuronal packaging, as assessed by DAPI staining; expression profiles of FoxP2, Ctip2, and Cux1; layer VI, V, and II–IV markers; and presumptive laminar architecture of *Foxg1*-GOF mutants (*Foxg1*$^{tTA/+}$;*TREt-Foxg1-IRES-Egfp*$^{+/-}$) versus *wt* controls (*Foxg1*$^{+/+}$;*TREt-Foxg1-IRES-Egfp*$^{-/-}$). (*B*) Comparative quantification of neocortical PV^{+} interneurons in neocortices of P35 *Foxg1* mutants and controls. Graphs show normalized densities of PV^{+} cells in *Foxg1*-GOF, *wt* (defined as in (*A*)) and *Foxg1*-LOF (*Foxg1*$^{tTA/+}$;*TREt-Foxg1-IRES-Egfp*$^{-/-}$) mice. Data refer to the dark gray region of the associated silhouettes. They are presented in a cumulative fashion (T, total) or are categorized along the medial–lateral axis (L, lateral; M, medial), the rostro-caudal axis (R, rostral; I, intermediate; C, caudal), and the radial axis (MZ, marginal zone; GM, gray matter; WM, white matter). (Absolute PV^{+} cell densities in *wt* animals are reported in Supplementary Table 1). Examples of anti-PV immunofluorescences refer to the boxed area within the intermediate frontal silhouette. Scale bars: 100 µm. (*C* and *D*) Comparative quantification of S100β^{+} astrocytes in P0 (*C*) and P7 (*D*) *Foxg1* mutants and controls. For both ages, graphs show *wt*-normalized densities of S100β^{+} cells in neocortices of *Foxg1*-GOF, *wt*, and *Foxg1*-LOF mice (genotypes defined as in (*A*)). Data refer to the dark gray region of the associated silhouettes. In case of P7 analysis, they are presented in a cumulative fashion (T, total) or are categorized along the medial–lateral axis (L, lateral; M, medial), the rostro-caudal axis (R, rostral; I, intermediate; C, caudal), and the radial axis (I, II–IV, V, VI, layers 1, 2–4, 5, 6; WM/SVZ, white matter/subventricular zone) (Absolute S100β^{+} cell densities in *wt* animals are reported in Supplementary Table 2). Examples of P0 and P7 anti-S100β and anti-EGFP immunofluorescences refer to the boxed areas within the corresponding silhouettes. Abbreviations: i–vi, layers I–VI; iz, intermediate zone; e, ependyma; *Foxg1*^{EGFP}, *TREt-Foxg1-IRES-EGFP* transgene-driven EGFP. Scale bars: 100 µm. Statistical significance evaluated by *t*-test (one-tailed, unpaired). *$P < 0.05$; **$P < 0.01$. *n* is the number of mice analyzed.

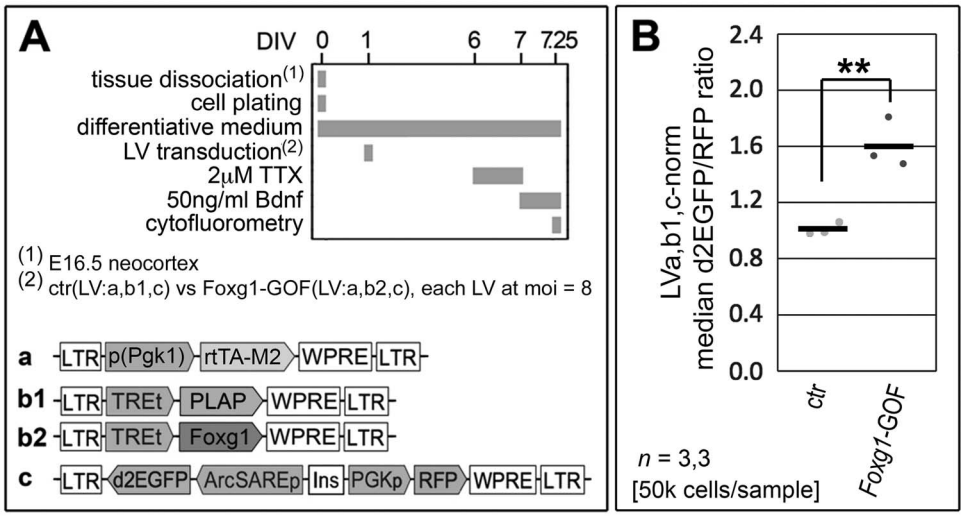

Figure 6. Evaluation of neocortical culture activity upon *Foxg1* overexpression, by delayed arc-promoter-driven-reporter fluorometry. Cytofluorimetric profiling of *Foxg1*-GOF, DIV7 cultures of dissociated E16.5 neocortical cells, harboring a d2EGFP activity reporter under the control of the "Arc-SARE-enhancer/minimal promoter (ArcSAREp)" neuronal activity-responsive element: (*A*) protocol and (*B*) results. The fluorescence ratio between the d2EGFP reporter and the constitutively expressed product of the cis-associated *PGKp-RFP* normalizer was determined per each cell and the median ratio of every biological replicate was plotted against its genotype. Horizontal bars, genotype averages. Data normalized against ctr values. Results evaluated by *t*-test (unpaired, one-tailed). $^{**}P < 0.01$. n = number of biological replicates, that is, independently transduced samples, each containing 50 000 cells.

neurons among total neurons; 2) occurrence of spontaneous Ca^{2+} episodes in active cells, evaluated by profiling cumulative distribution of inter-event intervals (IEIs, i.e., inter-calcium transients intervals); and 3) neuronal activity synchronization, by measuring cross-correlation factor (CCF) (Fig. 7*B*–*F*). The results were as follows.

We found that *Foxg1* knockdown reduced the prevalence of spontaneously active neurons (49% vs. 83%, with $P < 0.001$ and $n = 4,4$) (Fig. 7*B*, panel 3), as well as their CCF (0.14 ± 0.001 vs. 0.79 ± 0.002, with $P < 0.001$ and $n = 4,4$) (Fig. 7*B*, panel 5). Moreover, *Foxg1*-LOF cultures were characterized by transient high-frequency bursts of activity interspersed by prolonged silent periods (Fig. 7*B*, panel 2), resulting in a different cumulative distribution of IEIs ($P < 0.01$) (Fig. 7*B*, panel 4). In a few words, knocking down *Foxg1* caused a complex alteration in network dynamics, characterized by unevenly distributed calcium transients, restricted to less numerous hyposynchronized neurons.

As expected, generalized *Foxg1* overexpression conversely increased the prevalence of spontaneously active neurons (94% vs. 18%, with $P < 0.01$, $n = 3,3$) (Fig. 7*C*, panel 3), as well as their CCF (0.90 ± 0.04 vs. 0.19 ± 0.02, with $n = 3,1$) (Fig. 7*C*, panel 5), while prevalently shortening their IEIs ($P < 0.01$) (Fig. 7*C*, panel 4). This points to a strong functional impact of pan-neural *Foxg1* upregulation on synaptic networks, boosting neuronal activity.

Next, when *Foxg1* overexpression was limited to astrocytes, neither the prevalence of active neurons (29% vs. 30%, with $n = 5,4$) nor their CCF (0.9 ± 0.02 vs. 0.8 ± 0.02, with $n = 5,4$) was affected (Fig. 7*D*, panels 3, 5). Instead, IEIs were significantly increased ($P < 0.01$) (Fig. 7*D*, panel 4). This means that neuronal *Foxg1* upregulation is necessary to enhance network activity. It further suggests that *Foxg1*-GOF astrocytes may somehow dampen neuronal activity better than control astrocytes.

Conversely, restriction of *Foxg1* overexpression to the neuronal lineage increased the prevalence of active neurons (98% vs. 31%, with $P < 0.001$ and $n = 12,12$) (Fig. 7*E*, panel 3) and their CCF (0.98 ± 0.01 vs. 0.40 ± 0.01, with $P < 0.001$ and $n = 12,12$) (Fig. 7*E*, panel 5), while shifting cumulative distribution of IEIs significantly to the left ($P < 0.001$) (Fig. 7*E*, panel 4). This means that neuronal *Foxg1* upregulation is not only necessary but also sufficient to elicit a powerful stimulating effect on network activity.

Finally, further restriction of *Foxg1* overexpression to glutamatergic neurons increased the prevalence of active neurons and the frequency of calcium events, while not appreciably affecting the culture CCF (Fig. 7*F*). This suggests that interneuronal *Foxg1* upregulation may play a major role in network hypersynchronization.

Misregulation of *Foxg1*-GOF, Neocortical Neuron Transcriptome

To cast light on molecular mechanisms underlying overactivity of *Foxg1*-GOF neurons, we profiled the transcriptome of neuronal cultures originating from E16.5 neocortical precursors, transduced by a broadly expressed *Foxg1* transgene and allowed to age up to DIV8 in the presence of AraC. Four *Foxg1*-GOF and four control cultures were profiled. A minimum of 20 M paired reads/sample were collected and aligned against the reference genome, raw read counts were normalized as fragments per kilobase of exon model per million reads mapped (FPKM) values, and results were finally filtered according to standard procedures. Of ~53 000 genes, ~11 500 genes passed filtering. Among them, 5569 resulted to be differentially expressed in *Foxg1*-GOF versus control cultures (with $P < 0.05$ and FDR < 0.05). A total of 2837 were upregulated (763 of them >2-folds) and 2832 downregulated (665 of them >2-folds). As positive controls, total *Foxg1*-mRNA (quantified by *Foxg1*-cds-specific reads) was increased by 4.4-fold; *Arc* and *Hes1*, expected to robustly arise upon *Foxg1* overexpression (see Fig. 8 and Chiola et al. 2019), were upregulated as well, by 6.6-fold ($P < 5.31 \times 10^{-54}$, FDR < 2.53×10^{-52}) and 34.9-fold ($P < 1.12 \times 10^{-136}$, FDR < 2.93×10^{-134}), respectively; *Emx2* and *Tbr1*, normally dampened by *Foxg1*

A

assay [transgene configuration*]	E16.5 ncx cell plating	LV transd	2μM doxy	10μM AraC	Ca^{2+} profiling
Foxg1-LOF [(a1)-vs-(a2)]	DIV0	DIV1	----	DIV4-8	DIV8
Foxg1-GOF, generalized [(b1,c1)-vs-(b1,c3)]	DIV0	DIV1	DIV2-8	----	DIV8
Foxg1-GOF, astroglial [(b3,c1)-vs-(b3,c2)]	DIV0	DIV5	DIV6-10	----	DIV10
Foxg1-GOF, neuronal [(b2,c1)-vs-(b2,c2)]	DIV0	DIV1	DIV2-8	----	DIV8
Foxg1-GOF, neuronal-glutam [(b4,c1)-vs-(b4,c2)]	DIV0	DIV1	----	----	DIV8

* generally achieved via lentiviral transgene delivery to *wt* neural samples (each LV at moi=8); b4 intrinsically harbored by *Tg(Camk2a-tTA)*$^{+/-}$ neural samples.

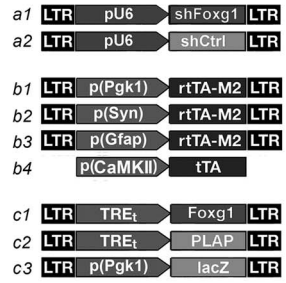

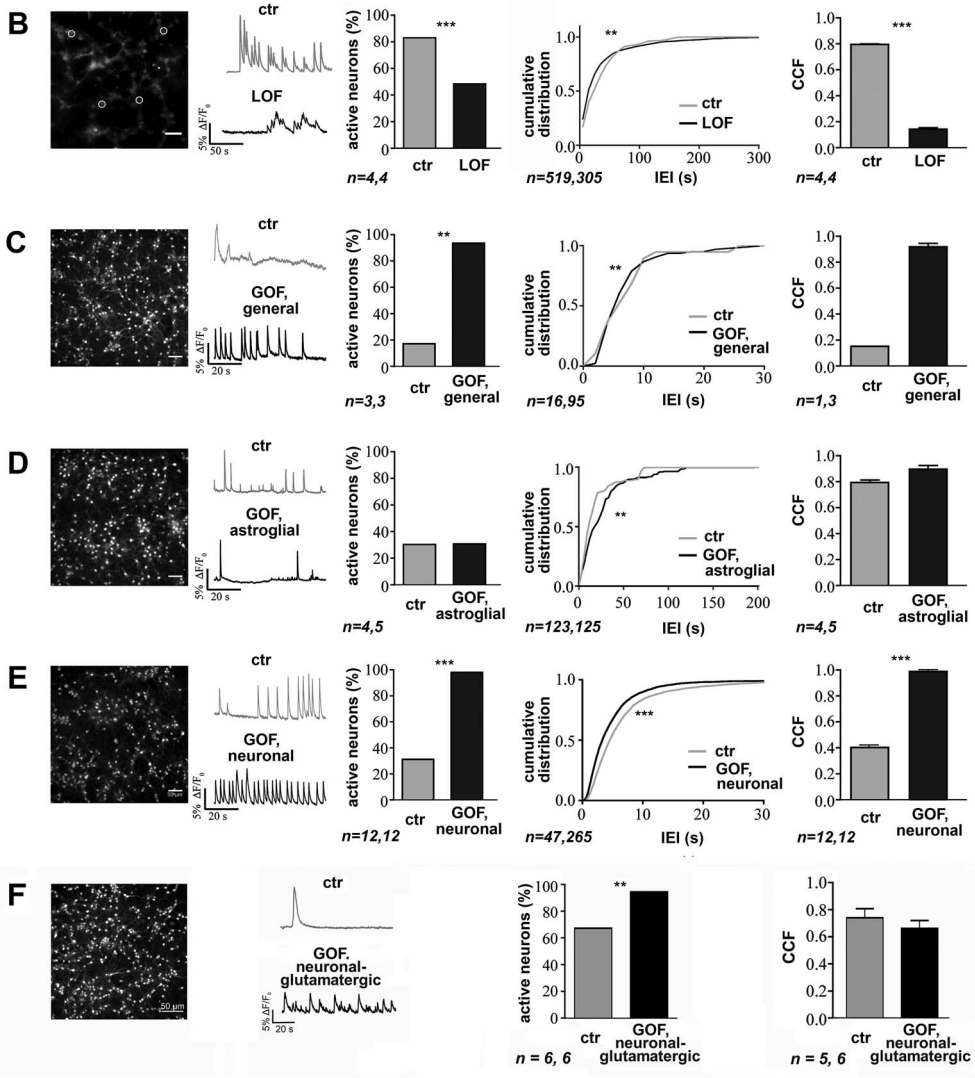

Figure 7. Evaluation of neocortical culture activity upon *Foxg1* expression level modulation, by real-time Ca^{2+} imaging. Ca^{2+} sensor-based, fluorimetric activity profiling of DIV8–10 cultures of dissociated E16.5 neocortical cells, loss- or gain of function (LOF or GOF) for *Foxg1*, and controls. (*A*) Experimental strategy, including transgene configurations employed. (*B–F*) Results, referring to LOF (B), as well as to generalized (*C*), astroglia-restricted (*D*), neuron-restricted (*E*), and glutamatergic neuron-restricted (*F*) GOF assays. In each (*B–F*) row, data presented as follows. In first panel (from left), snapshot of a representative field of manipulated *Foxg1* cultures, stained with Fluo4-AM (*B*) or Oregon-Green BAPTA 1-AM (*C–F*) Ca^{2+} indicators; scale bar: 50 μm. In second panel, examples of repetitive Ca^{2+} events spontaneously recorded from control (top) or *Foxg1*$^{LOF/GOF}$ (bottom) neurons. In third panel, the histogram represents percentages of spontaneously active cells in the two experimental contexts. In fourth panel, plot of cumulative IEI distributions in active cells of control (ctr) and *Foxg1*$^{LOF/GOF}$ cultures (omitted in case of (*F*), because of extremely low frequency of calcium events in controls, compared to actively discharging *Foxg1*-GOF samples). In fifth panel, the histogram summarizes the cross-correlation factor (CCF) measured under the two experimental conditions. Results evaluated by χ-squared test (spontaneously active neuron frequency), Kolmogorov–Smirnov assay (cumulative IEI distribution) and Mann–Whitney test (CCF). $^{**}P < 10^{-2}$, $^{***}P < 10^{-3}$. *n* represents: 1) the number of visual fields (each taken from an independently lentivirus-transduced cell sample) scored for assessment of "frequency of spontaneously active neurons" (third panel) and "CCF" (fifth panel) and 2) the number of active neurons inspected for evaluation of "cumulative IEI distribution" (fourth panel).

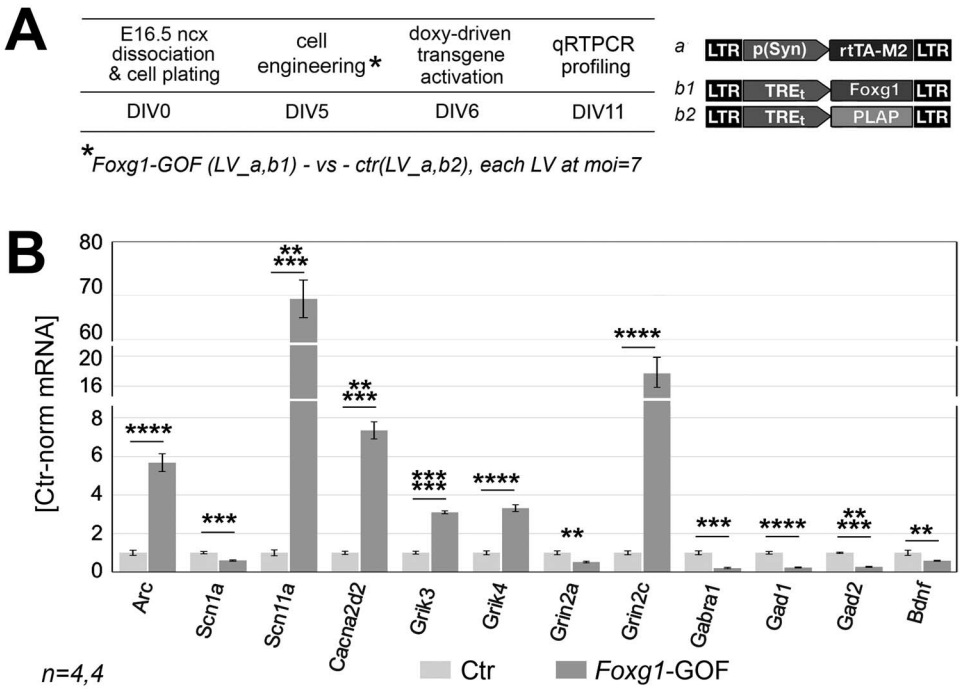

Figure 8. qRTPCR profiling of neocortical cultures overexpressing *Foxg1* in their neuronal compartment. (*A*) Protocol and (*B*) results. Data evaluated by *t*-test (unpaired, one-tailed). $^{**}P < 10^{-2}$, $^{***}P < 10^{-3}$, $^{****}P < 10^{-4}$, $^{*****}P < 10^{-5}$, $^{******}P < 10^{-6}$. *n* = number of biological replicates, that is, independently transduced cell samples.

(Muzio and Mallamaci 2005; Toma et al. 2014), were downregulated by −50.1% ($P < 1.26 \times 10^{-3}$, FDR $< 3.57 \times 10^{-3}$) and −14.5% ($P < 8.31 \times 10^{-3}$, FDR $< 1.93 \times 10^{-2}$), respectively (Supplementary Table 3 and Artimagnella and Mallamaci 2020).

Gene ontology (GO) terms enriched among differentially expressed genes included: actin cytoskeleton organization, axon guidance, ion transmembrane transport, potassium ion transport, calcium ion transport, vesicle-mediated transport, synaptic transmission (within the "biological process" class), dendrite, synapse, dendritic spine, postsynaptic membrane, synaptic vesicle, axon (within the "cellular component" class), ion channel activity, voltage-gated ion channel activity, potassium channel activity, calcium channel activity, PDZ domain binding, phosphatidylinositol binding, SH3 domain binding, integrin binding, protein tyrosine phosphatase activity, and phosphoprotein phosphatase activity (within the "molecular function" class). To get hints about molecular mechanisms underlying abnormal activity of *Foxg1*-GOF neurons, we specifically focused our attention on sets of differentially expressed genes linked to intracellular signal integration and synaptic transmission. Among them, genes encoding for: 1) plasma membrane, voltage-dependent ion channels, including those belonging to *Scn*, *Kcn*, and *Cacn* families (Catterall 2005; Johnston et al. 2010; Zamponi et al. 2010; Shah and Aizenman 2014), as well as pumps and channels mediating Ca^{2+} fluxes among cytoplasm, ER, mitochondria, and extracellular spaces (Kwon et al. 2016; Raffaello et al. 2016); 2) glutamatergic and GABAergic ionotropic receptors (Traynelis et al. 2010; Jembrek and Vlainic 2015; Crupi et al. 2019); 3) neuromodulator receptors (Gu 2002); and 4) selected structural components of synapses (Monteiro and Feng 2017). The results were highly articulated (Supplementary Table 3 and Artimagnella and Mallamaci 2020).

We found a widespread upregulation of *Scn* genes. *Scn1a*, mainly restricted to PV^+ interneurons and required for their inhibitory activity (Sun et al. 2016), was conversely decreased by about 4-fold. Quantification of *Kcn* genes did not show any simple shared trend. *Kcc2*, promoting the transition from gamma aminobutyric acid (GABA)-driven depolarization to hyperpolarization (Clayton et al. 1998; Rivera et al. 1999), was upregulated >3-fold. Members of *Cacna1*, *Cacnb*, and *Cacng* subfamilies were prevalently increased and the *Cacna2d2/Cacna2d1* ratio was specifically upregulated by about 28-fold, all pointing to a possible increase of *Cacn*-dependent Ca^{2+} currents (Dolphin 2016). A complex expression pattern was also displayed by other gene sets mastering Ca^{2+} exchanges among cytoplasm and other cell compartments. Implicated in Ca^{2+} extrusion to cell exterior, PMCA-encoding *Atp2b2–4* and NCX-encoding *Slc8a2,3* were upregulated and NCKX-encoding *Slc24a2,4* downregulated. SOCE effector-encoding genes *Stim1* and *Orai2*, promoting Ca^{2+} influx from cell exterior, were upregulated. Involved in release of ER Ca^{2+}, CICR- and IICR machinery genes *Ryr1,2* and *Itpr1,3* were downregulated and upregulated, respectively. SERCA-encoding *Atp2a2*, implicated in ER Ca^{2+} uptake, was downregulated. Finally, two repressors of the MCU machinery, mediating mitochondrial Ca^{2+} uptake, *Micu2* and *Micu3*, were downregulated, and its stimulator *Slc25a23* was upregulated, altogether prefiguring an increased activity of this machinery.

Next, genes encoding for ionotropic glutamatergic receptors showed a pattern definitively consistent with increased neocortical activity. *Grik1*, restricted to interneurons (Paternain et al. 2003), was downregulated; *Grik3*, active in pyramids and encoding for the principal GluK3 subunit (Wisden and Seeburg 1993), was upregulated; and *Grik4* and *Grik5*, both essential for the normal ionotropic function (Fernandes et al. 2009), were increased as well. As for *Gria* family, both *Gria2*, decreasing Ca^{2+} permeability of AMPA receptors, (Sanchez et al. 2001) and *Gria4*, needed to prevent epileptic seizures (Beyer et al. 2008), were downregulated. Finally, concerning *Grin* genes, in addition

to *Grin1* decline, *Grin2c*/*Grin2a* and *Grin2d*/*Grin2a* ratios were dramatically upregulated, pointing to likely prolonged opening times of NMDA receptors (Paoletti et al. 2013). *Grin3*, normally limiting Ca^{2+} permeability of these receptors (Wada et al. 2006), was downregulated. Moreover, a collapse of key genes implicated in GABAergic conduction and GABA-mediated homeostasis, *Gad1*, *Gad2*, *Gabra1*, *Bdnf* (Supplementary Fig. 9 and (Hong et al. 2008)), was also detected.

Dynamics of neuromodulator receptor genes (Gu 2002) was very complex. It included alterations with a potential pro-excitatory (*Chrnb4*, *Adra1b*, *Htr3a*, *Htr6,* and *P2rx4* upregulation, as well as *Grm2* and *Grm8* decline) or pro-inhibitory outcome (*Adra1a* and *P2rx2* downregulation as well as *Grm4* and *Drd2* upregulation). Similar considerations apply to modulation of structural synaptic genes, some upregulated (e.g., *Homer2*, *Nrxn2*,*3* and *Shank1*,*2*) and some decreased (e.g., *Homer1*, *Nlgn1*).

Remarkably, a misregulation of layer-specific genes was also evident (Supplementary Table 4). It included a widespread downregulation of layers 2–4, layer 6, and subplate markers and an upregulation of layer 5 ones, consistent with the laminar phenotype displayed by *Foxg1*-GOF mice (Fig. 5A and Supplementary Fig. 6 and Toma et al. 2014; Hou et al. 2019).

To strengthen these results, we evaluated mRNA levels of a subset of differentially expressed genes, in sister preparations of *Foxg1*-GOF cultures employed for Ca^{2+} imaging assays, by qRT-PCR. To note, here we restricted *Foxg1* overexpression to neurons, under the control of *pSyn* promoter. Moreover, we omitted AraC, so allowing neurons to mature in more biologically plausible conditions, for example, in the presence of a large astrocyte complement. Interestingly, qRTPCR analysis of these samples reproduced the variation pattern previously detected in RNASeq assays (*Scn11a*, *Grik3*, *Grik4, and Grin2c* upregulated, *Scn1a*, *Grin2a*, *Gabra1*, *Gad1*, *Gad2*, and *Bdnf* downregulated; Fig. 8), corroborating the scenario emerging from these assays.

To sum up, *Foxg1* upregulation in postmitotic neocortical neurons led to a misregulation of specific gene sets, encoding for layer-specific effectors as well as for voltage-gated Na^+ and Ca^{2+} ion channels, intracellular Ca^{2+} flux mediators, and glutamate- and GABA-gated ion channels. This misregulation points to a preferential promotion of layer 5 specification and prefigures a synergistic stimulation of neocortical activity.

Interneuron Depletion

We further wondered if, similar to our *Foxg1*-GOF mouse models, a misregulation of the GABAergic-to-glutamatergic neuron ratio could occur in *Foxg1*-GOF primary preparations, contributing to their abnormal activity profile. For this purpose, we set up cultures of E16.5 neocortical precursors originating from *Gad1*$^{EGFP/+}$ donors (Tamamaki et al. 2003), expressing EGFP in all GABAergic neurons; we engineered and processed them similarly to Fig. 7 assays; and we evaluated the resulting $EGFP^+NeuN^+/NeuN^+$ cell ratio at DIV8 (Fig. 9 and Supplementary Fig. 10). We found that generalized and neuron-restricted *Foxg1* overexpression, driven by *Pgk1* and *Syn* promoters, respectively, decreased this ratio from $16.8 \pm 0.6\%$ to $10.5 \pm 1.1\%$ ($P < 0.001$, $n = 4,4$) and from $10.6 \pm 0.4\%$ to $4.0 \pm 0.7\%$ ($P < 0.0001$, $n = 4,4$), respectively (Fig. 9B, graphs 2 and 4 from left). Astrocyte-confined *Foxg1* overexpression, under the control of the *Gfap*-promoter was ineffective (Fig. 9B, graph 3). Knockdown of endogenous *Foxg1* reduced this ratio only to a very limited extent, from $13.8 \pm 0.4\%$ to $12.7 \pm 0.4\%$ ($P < 0.04$, $n = 4,4$) (Fig. 9B, graph 1). In other words, a pronounced interneuron depletion takes place upon neuronal *Foxg1* upregulation, likely contributing to network hyperactivity evoked by this manipulation.

Activity-Dependent *Foxg1* Upregulation in Neocortical Neurons and Its Molecular Control

It is known that electrical activity exerts a complex impact on neuronal transcriptome (Kim et al. 2010). Therefore, we investigated whether, in addition to its ability to promote excitability, *Foxg1* would be in turn regulated by neuronal activity.

To address this issue, we transferred DIV6.5 neural cultures originating from E16.5 neocortical tissue under 25 mM extracellular K^+, namely a robust depolarizing treatment (He et al. 2011), and monitored temporal progression of *Foxg1*-mRNA and -protein (Fig. 10A). Both gene products underwent a substantial, transient upregulation. The former arose as early as at 1 h, peaked up at 3 h (about 2.75-fold), and later declined, getting back to baseline values by 18–24 h (Fig. 10C). The latter showed an appreciable increase already at 6 h, peaked up at around 12 h (about 1.75-fold), and later declined, rebounding to halved levels at about 24 h (Fig. 10D). Interestingly such positive correlation between *Foxg1* expression and neuronal activity was mainly restricted to hyperactive cultures, as neuron silencing by TTX downregulated *Foxg1*-mRNA only to a limited extent (Fig. 10B).

Looking for mechanisms underlying activity-dependent *Foxg1* regulation, we noticed that the *Foxg1* transcription unit and its surroundings are rich in binding sites for immediate early gene-encoded transcription factors (IEG-TFs), validated by Chromatin-Immuno-Precipitation (ChIP) in non-neural cell lines or predicted in silico by Jaspar software (Mathelier et al. 2014) (Fig. 11A). Therefore, we hypothesized that these TFs, including pCreb1, nuclear-$RelA^{p65}$, Fos, Egr1, Egr2 and Cebpb, might be instrumental in such regulation.

To test this prediction, first we checked if temporal progression of these TFs would be etiologically compatible with *Foxg1*-mRNA fluctuations, in primary neocortical cultures challenged by high potassium. Two of these effectors, pCreb1 and nuclear-Rel^{p65}, normally tuned by fast post-translational mechanisms (Flavell and Greenberg 2008; de la Torre-Ubieta and Bonni 2011; Sun et al. 2016), peaked up as early as at 20 min and remained above the baseline at least up to 90 min (Fig. 11C,E and Supplementary Fig. 11A,B). Consistently, the *d2EGFP*-mRNA products of the pCreb1- and NFkB-activity reporters cAMP.RE_3-p(min)-d2EGFP and NFkB.BS_4-p(min)-d2EGFP, pre-delivered to neural cells by lentiviral transgenesis (Fig. 10B), displayed also an early-onset, transient upregulation (Fig. 11D,F). Conversely, *Fos*-, *Egr1*-, *Egr2*-, and *Cebpb*-mRNAs, largely modulated by transcription-dependent mechanisms (Calella et al. 2007; Flavell and Greenberg 2008), peaked up at 1 h and then declined (Fig. 11G). In synthesis, activity-dependent elevation of all six effectors preceded *Foxg1*-mRNA induction. As such, this elevation could be instrumental in achieving *Foxg1* induction.

To corroborate this inference, we systematically knocked down all six IEG-TFs, by delivering the corresponding DN effectors (Supplementary Table 5) (Schwarz et al. 1996; Van Antwerp et al. 1996; Olive et al. 1997; Ahn et al. 1998; Park et al. 1999; Mayer et al. 2008) to primary neuronal cultures. We evaluated the impact of these manipulations, in basal conditions as well as upon culture exposure to 25 mM K^+ for 3 h. In particular, *Egr1* and *Egr2* were functionally co-silenced with a unique DN construct, Creb1-DN expression had to be set to very low levels to prevent neuronal damage (Fig. 12A). The majority of the DN

A

exp timing	E16.5 ncx dissociation & cell plating *	cell engineering: t	cell engineering: LVs	cell engineering: moi	2μg/mL doxy-driven transgene activation	profiling
Foxg1-LOF	DIV0	DIV2	(a1)-vs-(a2)	10	----	DIV8
Foxg1-GOF, generalized	DIV0	DIV2	(b1,c1)-vs-(b1,c3)	8+8	DIV3	DIV8
Foxg1-GOF, astroglial	DIV0	DIV5	(b3,c1)-vs-(b3,c2)	8+8	DIV6	DIV8
Foxg1-GOF, neuronal	DIV0	DIV2	(b2,c1)-vs-(b2,c2)	8+8	DIV3	DIV8

* from $Gad1^{EGFP/+}$ donors

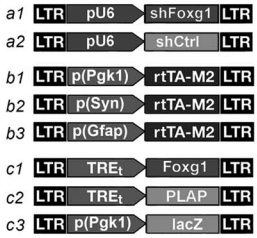

B

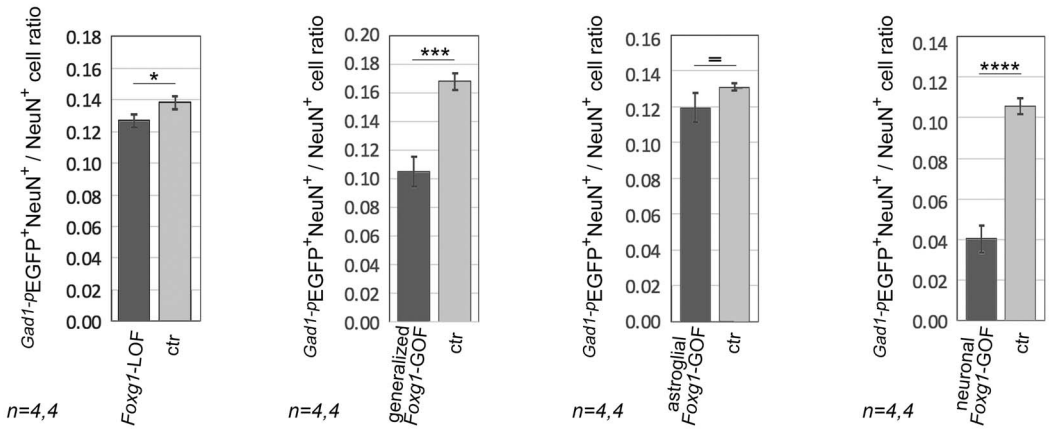

Figure 9. Interneuron quantification in *Foxg1*-GOF neocortical cultures. (*A*) Protocol and lentiviruses employed and (*B*) results. Data evaluated by *t*-test (unpaired, one-tailed). $^{*}P < 0.05$, $^{**}P < 10^{-2}$, $^{****}P < 10^{-4}$. *n* = number of biological replicates, that is, independently transduced cell samples.

devices employed downregulated *Foxg1*-mRNA by about 15–40%, both in baseline conditions and in the presence of 25 mM K^+. NFkB-DN was specifically ineffective under high K^+. Creb1-DN conversely reduced *Foxg1*-mRNA by about 50% and 90%, in baseline condition and under high K^+, respectively (Fig. 12B, 1st and 3rd graphs). Altogether, these results suggest that all six IEG-TFs under analysis contribute to sustain neuronal *Foxg1* transcription, synergically and to various extents, in resting conditions as well as following intense electrical activity. In particular, they point to pCreb1 as a key player in this context.

Finally, inspired by the presence of a number of known *Foxg1*-binding sites within the *Foxg1* locus (Fig. 11A and data not shown), we further speculated that late decrease of *Foxg1* gene products upon prolonged K^+ stimulation (Fig. 10C,D) did not simply reflect the delayed decline of its transactivators, but it could be enhanced by *Foxg1* self-inhibition. As expected, the delivery of a neuron-restricted *Foxg1* transgene (Fig. 12A) downregulated endogenous *Foxg1* by >80%, both in the absence of K+ stimulation and under high K^+ (Fig. 12B, 2nd and 4th graphs). Consistently, the same transgene robustly shifted the *Foxg1*(*t*) expression curve downward in aging neocortical cultures (Supplementary Fig. 12A,B).

Summing up, neuronal hyperactivity elicited a delayed and transient upregulation of *Foxg1* mRNA and protein, mediated by the products of IEGs as well as by the negative feedback exerted by the *Foxg1* protein on its encoding gene.

Hyperactivation of IEGs in K^+-Stimulated, *Foxg1*-GOF Neocortical Cultures

Hyperactivity of *Foxg1*-GOF neocortical cultures and activity-dependent *Foxg1* upregulation suggest that a reciprocal positive feedback may take place between *Foxg1* overexpression and neocortical activity. This feedback might finely tune neocortical activity of healthy individuals and strengthen electroclinical signs of those with increased *Foxg1* dosage.

To test this prediction in a more stringent and biologically plausible context, *Foxg1* was upregulated by gentle RNAa (Fig. 13A), eliciting a 1.5×–2.0× expression gain, presumably close to that caused by *FOXG1* duplications, and complying with activity-dependent gene tuning (Fimiani et al. 2016). Then, neural cultures were pulsed by high K^+ and profiled for activity and expression of selected IEGs (Fig. 13A), as proxies of ongoing neuronal activity (Flavell and Greenberg 2008) and—meanwhile—promoters of it (Jones et al. 2001; Lopez de Armentia et al. 2007; Jancic et al. 2009; Viosca et al. 2009; Gruart et al. 2012; Penke et al. 2013; Koldamova et al. 2014).

Interestingly, following K^+ stimulation, the *d2EGFP*-mRNA product of the pCreb1-activity reporter was rapidly upregulated in *Foxg1*-GOF samples compared to controls ($ctr_{t=0}$-normalized levels at 1 h were 1.74 ± 0.11 vs. 1.36 ± 0.13, respectively, with $P < 0.032$) (Fig. 13B, left graph). The corresponding NFkB-activity reporter, similarly upregulated at 50 min in *Foxg1*-GOF samples and controls (1.15 ± 0.03 and 1.19 ± 0.12, respectively, with $P = 0.296$), retained its overexpression at 2 h in the former, while declining in the latter (1.22 ± 0.14 vs. 0.94 ± 0.08, with $P < 0.003$) (Fig. 13B, right graph).

A consistent scenario emerged from quantification of endogenous *Fos*, *Egr1*, and *Cebpb*-mRNAs. Peaking at 1 h in *Foxg1*-GOF samples like in controls, both *Fos*- and *Egr1*-mRNAs showed a delayed rebound toward baseline in *Foxg1*-GOF samples compared to controls ($ctr_{t=0}$-normalized levels at 2 h were 62.3 ± 2.68 vs. 48.87 ± 3.91, with $P < 0.015$, and 24.88 ± 4.40 vs. 16.65 ± 1.78, with $P < 0.049$, respectively) (Fig. 13C). *Cebpb*-mRNA

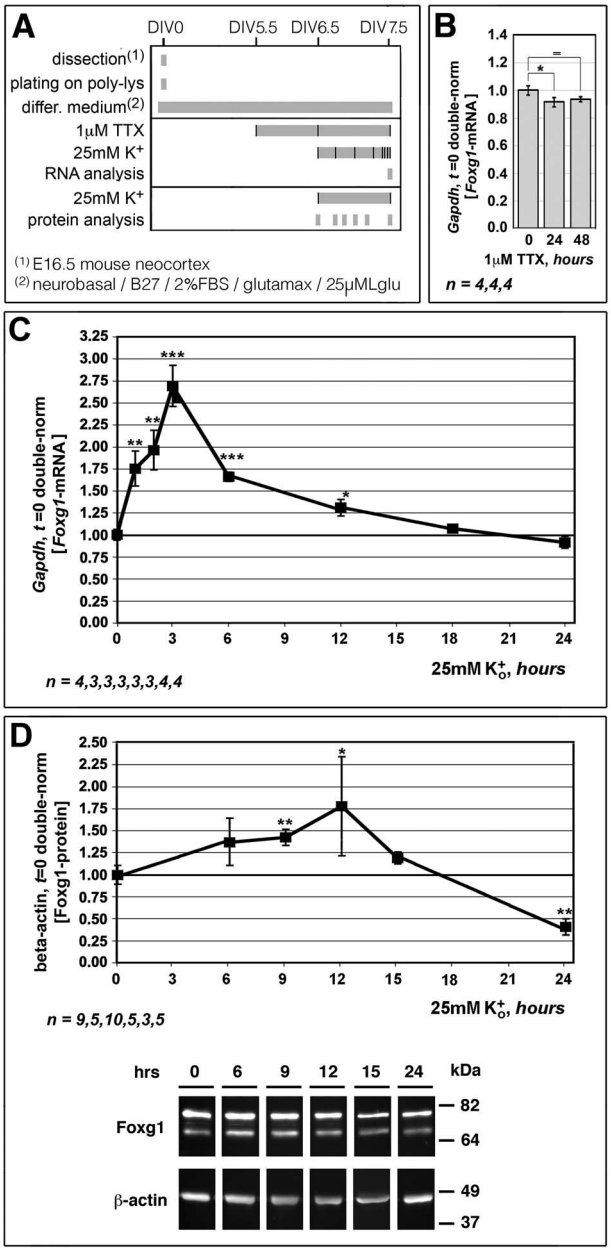

Figure 10. Activity-dependent modulation of neocortical *Foxg1* expression. Evaluation of *Foxg1* expression levels in dissociated DIV7 cultures originating from E16.5 neocortical tissue: protocol (*A*) and results (*B–D*). In (*B*, *C*) qRTPCR quantification of *Foxg1*-mRNA in cultures silenced by 1 μM TTX for 0–48 h (*B*) or stimulated by 25 mM K^+ for 0–24 h (*C*). In (*D*) WB quantification of *Foxg1*-protein in cultures stimulated by 25 mM K^+ for 1–24 h. Data double normalized, against *Gapdh* (*B*, *C*) or beta-actin (*D*), and $t=0$ baseline values (*B–D*). Results evaluated by *t*-test (unpaired, one-tailed), run against $t=0$ values. $^*P<0.05$, $^{**}P<0.01$, $^{***}P<0.001$. n = number of biological replicates, that is, independently grown cell samples.

was conversely upregulated in *Foxg1*-GOF samples for at least 6 h after high K^+ exposure (for example, $ctr_{t=0}$-normalized levels at 2 h were 4.96 ± 0.39 and 3.64 ± 0.24, in GOF and ctr samples, respectively, with $P < 0.016$) (Fig. 13C).

Altogether, these data confirm that an even mild *Foxg1* overexpression, comparable to that occurring in healthy hyperactive neurons or in human patients with a supranumerary *FOXG1* allele, might enhance and/or lengthen neocortical responses to depolarizing stimuli, a phenomenon of remarkable physiopathological interest.

Discussion

To cast light on the impact of *Foxg1* on neocortical neuronal activity, we took advantage of a novel transgenic mouse model, overexpressing this gene within deep neocortical pyramids (Fig. 1). Transgenic animals showed an abnormal EEG (Fig. 3) and resulted more prone to KA-evoked limbic motor seizures (Fig. 4). A pronounced hyperactivity of neocortical neurons underlay such phenotype (Figs 2 and 4D). A prominent interneuron reduction throughout gray matter as well as an astroglial deficit mainly confined to lateral superficial neocortex (Fig. 5) likely contributed to it. Remarkably, *Foxg1* overexpression achieved by lentiviral transgene delivery to dissociated, neocortical neurons also increased their activity and synchronization (Figs 6 and 7). Looking for underlying molecular mechanisms, we profiled the transcriptome of these cells. Results of this analysis included: an upregulation of large *Scn* and *Cacn* gene sets, encoding for Na^+ and Ca^{2+} channels; complex anomalies in other key genes governing Ca^{2+} fluxes; aberrancies in *Grin*, *Gria*, and *Grik*, NMDA-, AMPA-, and KA-receptor genes; as well as a collapse of the GABAergic axis, including *Gad1*, *Gad2*, *Gabra1*, and *Bdnf* (Fig. 8 and Supplementary Table 3). Moreover, we investigated if neuronal activity would—in turn—regulate *Foxg1* expression. We found an activity-driven transient upregulation of this gene (Fig. 10), mediated by the products of IEGs (Figs 11 and 12). This points to a positive feedback between *Foxg1* and neuronal activity (Fig. 13), likely tuning neocortical function of healthy individuals and driving neurological aberrancies of patients with altered *Foxg1* dosage.

Originally conceived to achieve pan-telencephalic *Foxg1* overexpression, the transgene employed in in vivo assays resulted to be confined to postmitotic, deep neocortical pyramids (Fig. 1 and Supplementary Figs 2–4). This likely reflected transgene integration into a particular genomic location, permissive to transcription only in these cells (Pikaart et al. 1998). Albeit unexpected, this offered us the serendipitous opportunity to specifically explore the role exerted by our gene of interest in such cells, in living mice. As the hippocampus of these animals did not express the transgene, its spontaneous electroclinical signs and KA-evoked hyperactivity were hardly autochthonous. Rather, they reflected abnormal neocortical inputs fed into this structure, which could be so exploited as an in vivo proxy of the neocortical phenotype.

As expected, an increase of neocortical projection neurons activity was actually detectable. This increase was primarily inferred in neocortical derivatives of *Foxg1*-GOF transgenic embryos, by pErk1 and *cfos*-RNA activity-responsive reporters (Tyssowski et al. 2018) (Figs 2 and 4D and Supplementary Fig. 5). It was later confirmed in neocortical neurons made *Foxg1*-GOF via somatic lentiviral transgenesis, by Arc-SARE activity reporter (Kawashima et al. 2009) and optical profiling of Ca^{2+} indicators (Figs 6 and 7). Remarkably, the positive correlation between *Foxg1* expression levels and neuron network synchronization emerged following generalized, both GOF and LOF *Foxg1* manipulations. Furthermore, neuronal hyperactivity was still prominent when *Foxg1* overexpression was restricted to glutamatergic neurons (Figs 1 and 7F and Supplementary Fig. 2–4), pointing to mechanisms mostly taking place in these cells.

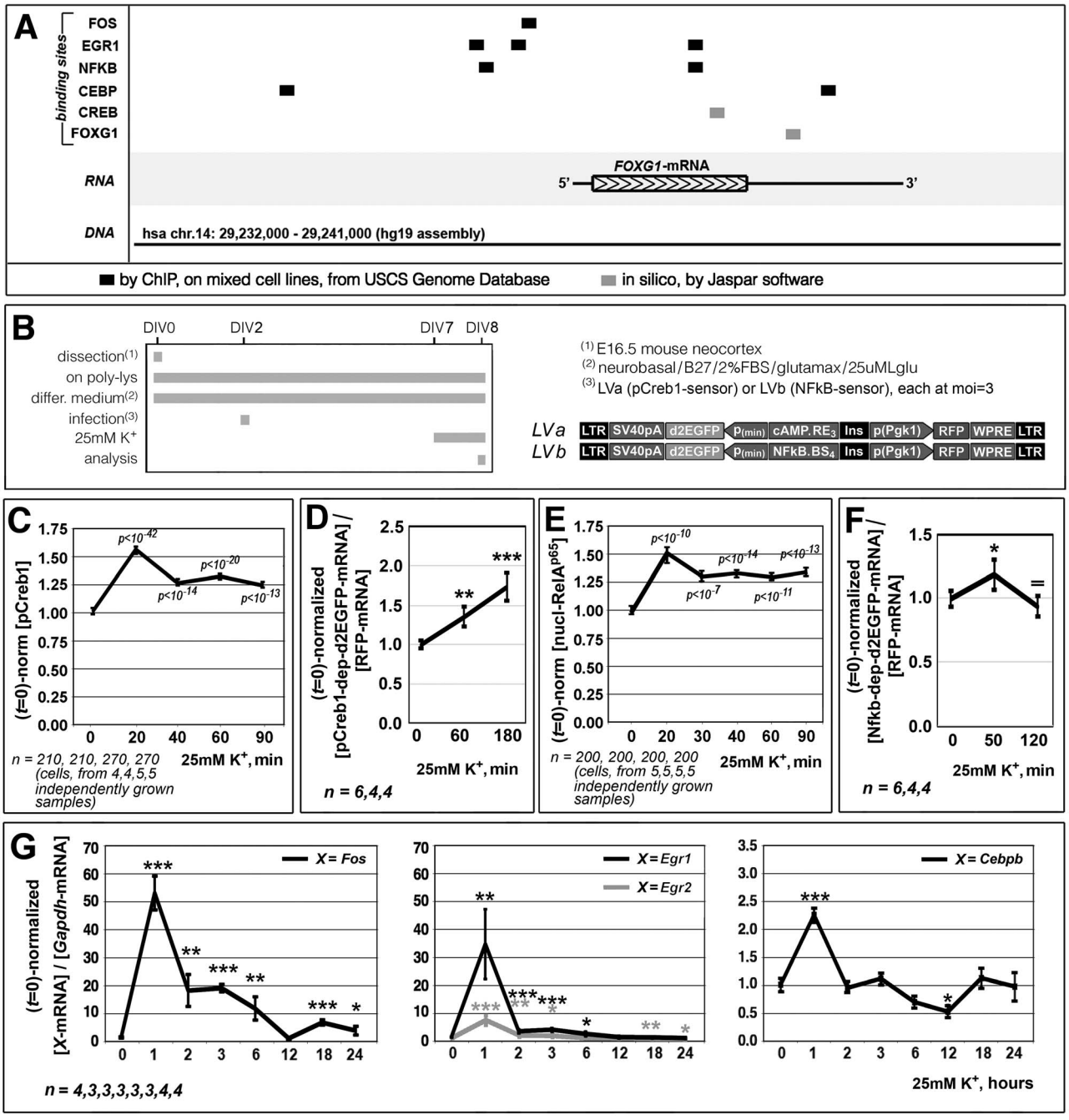

Figure 11. Selecting putative mediators of *Foxg1* response to high K^+. (*A*) Localization of IEGF- (immediate early gene factor) and *Foxg1*-BSs (binding sites) within the *Foxg1* locus, as detected by ChIP on selected cell lines (UCSC) or predicted by Jaspar software. (*B–G*) Fluctuations of select IEGFs levels and activities evoked by timed exposure of dissociated DIV7 cultures originating from E16.5 neocortex to 25 mM K^+: (*B*) protocol and (*C–G*) results. As for *Creb*1, shown are (C) qIF (quantitative immunofluorescence) evaluation of phosphoprotein level and (*D*) qRTPCR evaluation of its pro-transcriptional activity, in cultures stimulated by 25 mM K^+ for up to 180 min (activity reporter: *d2EGFP*-mRNA product of the cAMP.RE_3-p(min)-d2EGFP transgene). Concerning $RelA^{p65}$, shown are (*E*) qIF evaluation of nuclear protein level and (*F*) qRTPCR evaluation of its pro-transcriptional activity, in cultures stimulated by 25 mM K^+ for up to 120 min (activity reporter: *d2EGFP*-RNA product of the NFkB.BS_4-p(min)-d2EGFP transgene). As for *Fos*, *Egr1*, *Egr2*, and *Cebpb*, shown is (*G*) qRTPCR evaluation of endogenous mRNA levels in cultures stimulated by 25 mM K^+ for up to 24 h. Data normalized against (*C*, *E*) $iegF_{t=0}$; (*D*, *F*) *RFP*-$mRNA_{t=ti}$ and (*d2EGFP*-mRNA/*RFP*-mRNA)$_{t=0}$ (*RFP*-mRNA as the product of the *p*(*Pgk1*)-*RFP* transgene); (*G*) *Gapdh*-$mRNA_{t=ti}$ and (*iegF*-mRNA/*Gapdh*-mRNA)$_{t=0}$. Results evaluated by *t*-test (unpaired, one-tailed), run against $t=0$ values. *$P<0.05$, **$P<0.01$, ***$P<0.001$. n = number of biological replicates, that is, (*D*, F, *G*) independently in vitro grown cell samples, or (*C*, *E*) individual neural cells, evenly and randomly taken from the reported number of independently transduced samples.

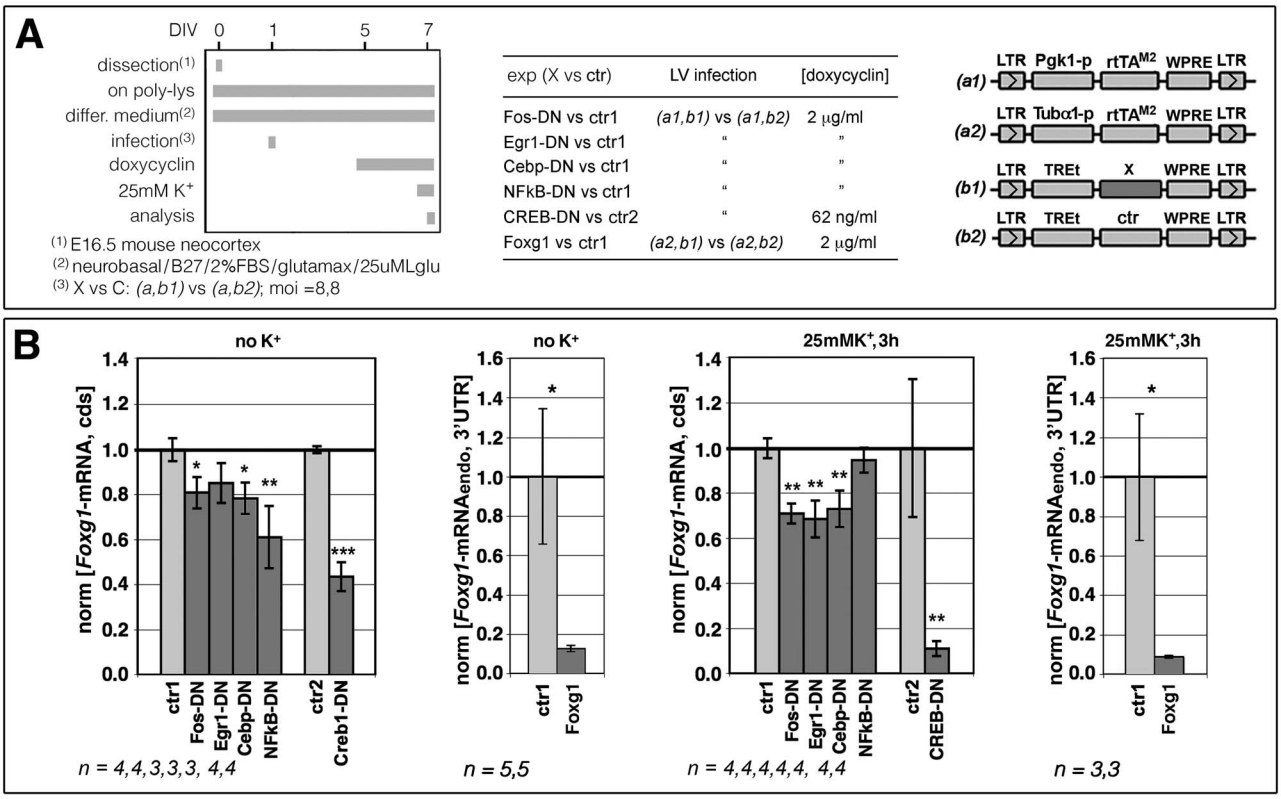

Figure 12. Validating putative mediators of *Foxg1* response to high K^+. *Foxg1* regulation in primary neocortical cultures engineered by immediate early gene-dominant negative (*IEG-DN*) or *Foxg1* transgenes: (*A*) protocol and (*B*) results. In (*B*), endogenous-*Foxg1*-mRNA levels upon expression of *IEG-DNs* or exogenous *Foxg1*, in the presence of physiological $[K^+]_o$ ("no K^+") or under 25 mM $[K^+]_o$, are shown. *Foxg1*-cds and *Foxg1*–3′UTR amplicons were used as proxies of endogenous *Foxg1* transcripts in graphs 1, 3 and 2, 4, respectively. ctr is *Plap*. Data double normalized, against *Gapdh*-mRNA and ctr samples. Results evaluated by *t*-test (unpaired, one-tailed). $^*P < 0.05$, $^{**}P < 0.01$, $^{***}P < 0.001$. *n* = number of biological replicates, that is, independently transduced cultures.

Concerning molecular mechanisms underlying such phenotype, RNA profiling of *Foxg1*-GOF cultures highlighted pronounced alterations of different specific gene sets, likely contributing to it (Fig. 8 and Supplementary Table 3). General dynamics of *Scn* and *Cacn* genes, as well as changes in NCKX, SOCE, IICR, and SERCA genes, prefigure neuron hyperexcitability. Misregulation of MCU genes, likely enhancing mitochondrial Ca^{2+} uptake, might stimulate respiration and sustain enduring electrical activity (Sanganahalli et al. 2013). Unbalanced expression of *Gria*, *Grik*, and *Grin* genes might result into strengthened glutamatergic conduction. Last but not least, the collapse of *Gad* and *Scn1a* genes as well as the decline of *Gabra1* and *Bdnf* might jeopardize GABAergic control of neocortical circuits. An ad hoc follow-up work will be required to rigorously test these predictions.

To note, two concomitant histological abnormalities characterizing the neocortex of *Foxg1*-GOF mutants, a widespread decrease of interneurons and a more localized astroglial deficit (Fig. 5B–D), might have worsened their phenotype. Both phenomena originated noncell autonomously, as neither interneurons nor astrocytes expressed the transgene (Fig. 1E,F). A prominent reduction of GABAergic interneuron prevalence also occurred in neocortical cultures made *Foxg1*-GOF by somatic lentiviral transgenesis (Fig. 9 and Supplementary Fig. 9).

Remarkably, we also found that *Foxg1*-mRNA was transiently upregulated under high $[K^+]_O$ and slightly downregulated upon TTX administration, suggesting that its levels are physiologically sensitive to changes of electric activity (Fig. 10C). An upregulation of *Foxg1* protein followed the mRNA peak, corroborating its potential relevance (Fig. 10D). Intriguingly, bioinformatic inspection of the *Foxg1* locus revealed a number of binding sites for immediate early factors. As expected (Calella et al. 2007; Flavell and Greenberg 2008; Snow and Albensi 2016), some of them (or their mRNAs) showed a pronounced upregulation, which preceded the *Foxg1*-mRNA maximum at 3 h. Specifically, pCreb1 and nuclear-Nfkb peaked at 20 min, *Fos*-, *Egr1*-, *Egr2*- and *Cebpb*-mRNAs at about 1 h (Fig. 11 and Supplementary Fig. 11). Their functional knockdown, by dominant negative devices, generally reduced *Foxg1*-mRNA both in basal conditions and under high $[K^+]_o$ (Fig. 12). These data point to an involvement of these effectors in mediating the impact of electric activity on *Foxg1* levels. Finally, the introduction of an exogenous *Foxg1* transgene dampened the expression of its endogenous counterpart, suggesting that an autologous negative feedback may restrict activity-dependent *Foxg1* arousal (Fig. 12).

In summary, *Foxg1* expression promotes neocortical electrical activity which, in turn, may stimulate *Foxg1* expression. This feedback suggests a crucial *Foxg1* role in fine-tuning of neocortical excitability. In this respect, progressive postnatal decline of *Foxg1* levels (Supplementary Fig. 12) might contribute to reduced excitability of more aged brains and misregulation of *Foxg1*-mRNA in patients with *Foxg1* copy number variations might deeply affect neuronal activity, resulting in their Rett-like- and West-like EEG aberrancies (Florian et al. 2011; Seltzer

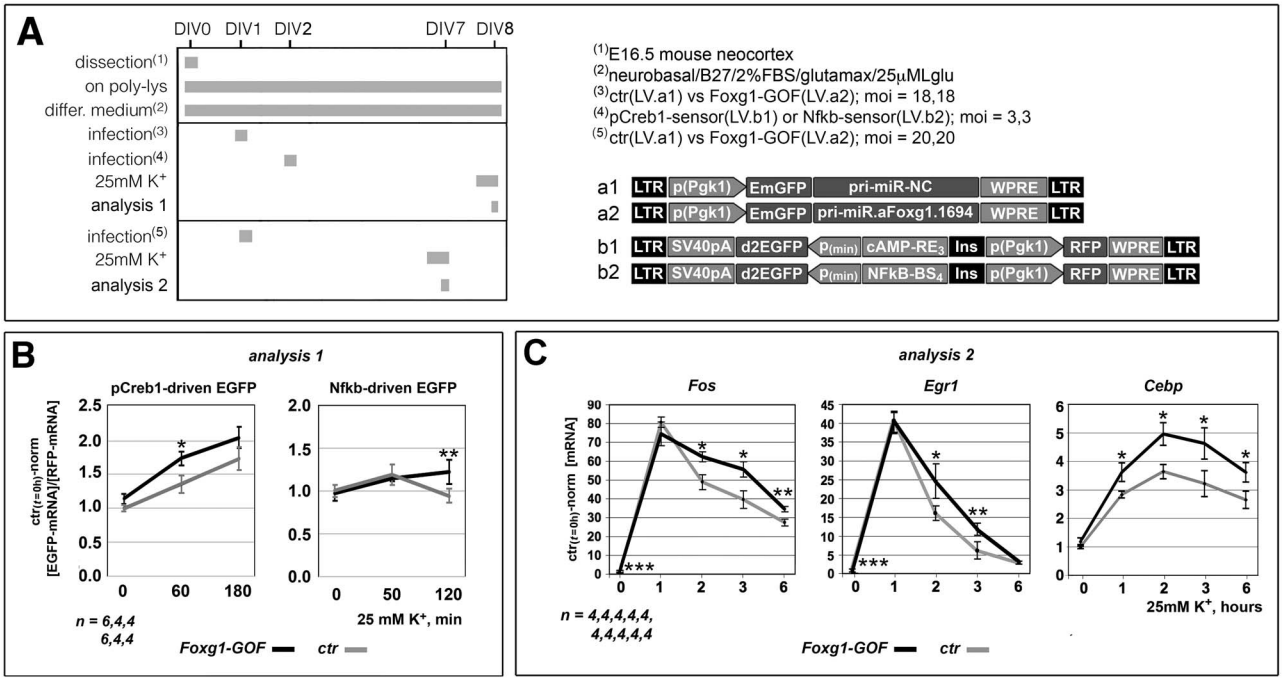

Figure 13. *Foxg1*-driven modulation of ieg response to high K^+. Activities and expression levels displayed by select IEG proteins and mRNAs, respectively, in dissociated, lentivector-engineered E16.5 + DIV7 neocortical cultures, upon chronic *Foxg1* upregulation via RNA activation (RNAa) and timed culture exposure to 25 mM K^+: protocol (*A*) and results (*B*, *C*). In (*B*), qRTPCR evaluation of pCreb1 and NFkb transcriptional activities; proxies: *d2EGFP*-mRNA products of lentiviral cAMP.RE_3-p(min)-d2EGFP and NFkB.BS_4-p(min)-d2EGFP transgenes, respectively. (*C*), qRTPCR evaluation of *Fos*, *Egr1*, *Egr2*, and *Cebpb* mRNA levels. Data normalized against (*B*) *RFP*-$mRNA_{t=ti}$ and (*d2EGFP*-mRNA/*RFP*-mRNA)$_{t=0}$ [*RFP*-mRNA product of the lentiviral p(Pgk1)-RFP transgene] and (*C*) *Gapdh*-$mRNA_{t=ti}$ and (*IEGF*-mRNA/*Gapdh*-mRNA)$_{t=0}$. Results evaluated by *t*-test (unpaired, one-tailed), run against $ctr_{t=ti}$ values. $^*P < 0.05$, $^{**}P < 0.01$, $^{***}P < 0.001$. *n* = number of biological replicates, that is, independently transduced cell samples.

et al. 2014). Consistently, gentle stimulation of *Foxg1* by saRNAs led to a complex upward distortion of fluctuations of pCreb1 and Nfkb activity, as well as of *Fos*-, *Egr1*-, and *Cebp*-mRNAs, evoked by high $[K^+]_o$ (Fig. 13). Non mere indices of neuronal hyperactivity, upregulation of pCreb1, Egr1 and Fos *may promote* neuronal hyper-activity and -excitability (Jones et al. 2001; Lopez de Armentia et al. 2007; Jancic et al. 2009; Viosca et al. 2009; Zhou et al. 2009; Yassin et al. 2010; Descalzi et al. 2012; Gruart et al. 2012; Penke et al. 2013; Koldamova et al. 2014; Ryan et al. 2015). Functional relevance of these phenomena to *Foxg1*-associated phenotypes will be subject of a dedicated follow-up study.

Supplementary Material

Supplementary material is available at *Cerebral Cortex* online.

Author Contributions

W.T. contributed to study of activity-dependent *Foxg1* regulation, investigated *Foxg1*-dependent regulation of interneurons and IEGs, and contributed to transcriptomic profiling of *Foxg1*-GOF cultures, Ca^{2+} imaging studies, and manuscript writing. M.P. took care of generation and histological characterization of *Foxg1*-GOF mice, contributed to investigate their KA-susceptibility, and investigated molecular control of activity-dependent *Foxg1* regulation. O.A. took care of pErk profiling of neuronal activity, transcriptomic profiling of *Foxg1*-GOF cultures, and study of activity-dependent *Foxg1* regulation and contributed to manuscript revision. M.S. took care of pErk and ArcSARE profiling of neuronal activity, set up astrocyte-confined transgene expression, and contributed to Ca^{2+} imaging assays and manuscript revision. R.R. took care of Ca^{2+} imaging, analyzed Ca^{2+} imaging data, and contributed to write the manuscript. T.S. and F.P.S.U. took care of Ca^{2+} imaging assays. G.P. took care of KA susceptibility assays and in situ hybridization profiling of KA-treated brains. M.A. took care of in vivo EEG analysis. M.C. supervised EEG studies. L.B. supervised Ca^{2+} imaging studies. Y.B. supervised KA susceptibility and in situ hybridization studies. A.M. designed this study, supervised its execution and wrote the manuscript.

Funding

Telethon Italy (grant GGP13034 to A.M.); Fondation Jerome Lejeune (grant 1621-MA2017A to A.M.); International FOXG1 Research Foundation (grant to A.M.); SISSA (intramurary funding to A.M. and YounGrant R_SSA-ALTR_YG_PS18_20_NEUR_ref_gruppo_0477 to R.R., T.S., M.S., and W.T.).

Notes

We thank 1) Marco Brancaccio, for early assessment of *Tg:Tre-Foxg1-IRES-Egfp*$^{+/-}$ transgenic lines; 2) Clara Grudina, for early setting up of protocols for Arc-SARE profiling of neuronal activity; and 3) Elisa Piscianz, for technical help with cytofluorometry. *Conflict of Interest*: The authors declare no competing interests.

References

Ahn S, Olive M, Aggarwal S, Krylov D, Ginty DD, Vinson C. 1998. A dominant-negative inhibitor of CREB reveals that it is a general mediator of stimulus-dependent transcription of c-fos. *Mol Cell Biol*. 18:967–977.

Artimagnella O, Mallamaci A. 2020. RNASeq profiling of *Foxg1*-GOF neocortical neurons.v2. *Zenodo*. doi: 10.5281/zenodo.3739467.

Beyer B, Deleuze C, Letts VA, Mahaffey CL, Boumil RM, Lew TA, Huguenard JR, Frankel WN. 2008. Absence seizures in C3H/HeJ and knockout mice caused by mutation of the AMPA receptor subunit Gria4. *Hum Mol Genet*. 17:1738–1749.

Bosi S, Rauti R, Laishram J, Turco A, Lonardoni D, Nieus T, Prato M, Scaini D, Ballerini L. 2015. From 2D to 3D: novel nanostructured scaffolds to investigate signalling in reconstructed neuronal networks. *Sci Rep*. 5:9562.

Brancaccio M, Pivetta C, Granzotto M, Filippis C, Mallamaci A. 2010. Emx2 and Foxg1 inhibit gliogenesis and promote neuronogenesis. *Stem Cells*. 28(7):1206–1218.

Calella AM, Nerlov C, Lopez RG, Sciarretta C, von Bohlenund Halbach O, Bereshchenko O, Minichiello L. 2007. Neurotrophin/Trk receptor signaling mediates C/EBPalpha, −beta and NeuroD recruitment to immediate-early gene promoters in neuronal cells and requires C/EBPs to induce immediate-early gene transcription. *Neural Dev*. 2:4.

Catterall WA. 2005. International Union of Pharmacology. XLVII. Nomenclature and structure-function relationships of voltage-gated sodium channels. *Pharmacol Rev*. 57:397–409.

Chiola S, Do MD, Centrone L, Mallamaci A. 2019. Foxg1 overexpression in neocortical pyramids stimulates dendrite elongation via Hes1 and pCreb1 upregulation. *Cereb Cortex*. 29(3):1006–1019.

Clayton GH, Owens GC, Wolff JS, Smith RL. 1998. Ontogeny of cation-cl- cotransporter expression in rat neocortex. *Brain Res Dev Brain Res*. 109:281–292.

Crupi R, Impellizzeri D, Cuzzocrea S. 2019. Role of metabotropic glutamate receptors in neurological disorders. *Front Mol Neurosci*. 12:20.

de la Torre-Ubieta L, Bonni A. 2011. Transcriptional regulation of neuronal polarity and morphogenesis in the mammalian brain. *Neuron*. 72:22–40.

Descalzi G, Li X-Y, Chen T, Mercaldo V, Koga K, Zhuo M. 2012. Rapid synaptic potentiation within the anterior cingulate cortex mediates trace fear learning. *Mol Brain*. 5:6.

Dolphin AC. 2016. Voltage-gated calcium channels and their auxiliary subunits: physiology and pathophysiology and pharmacology: voltage-gated calcium channels. *J Physiol*. 594:5369–5390.

Falcone C, Santo M, Liuzzi G, Cannizzaro N, Grudina C, Valencic E, Peruzzotti-Jametti L, Pluchino S, Mallamaci A. 2019. Foxg1 antagonizes neocortical stem cell progression to Astrogenesis. *Cereb Cortex*. 29(12):4903–4918.

Fernandes HB, Catches JS, Petralia RS, Copits BA, Xu J, Russell TA, Swanson GT, Contractor A. 2009. High-affinity Kainate receptor subunits are necessary for ionotropic but not metabotropic signaling. *Neuron*. 63:818–829.

Fimiani C, Goina E, Su Q, Gao G, Mallamaci A. 2016. RNA activation of haploinsufficient Foxg1 gene in murine neocortex. *Sci Rep*. 6:39311.

Flavell SW, Greenberg ME. 2008. Signaling mechanisms linking neuronal activity to gene expression and plasticity of the nervous system. *Annu Rev Neurosci*. 31:563–590.

Florian C, Bahi-Buisson N, Bienvenu T. 2011. FOXG1-related disorders: from clinical description to molecular genetics. *Mol Syndromol*. 2(3–5):153–163.

Gruart A, Benito E, Delgado-Garcia JM, Barco A. 2012. Enhanced cAMP response element-binding protein activity increases neuronal excitability, hippocampal long-term potentiation, and classical eyeblink conditioning in alert behaving mice. *J Neurosci*. 32:17431–17441.

Gu Q. 2002. Neuromodulatory transmitter systems in the cortex and their role in cortical plasticity. *Neuroscience*. 111:815–835.

Hanashima C, Fernandes M, Hebert JM, Fishell G. 2007. The role of Foxg1 and dorsal midline signaling in the generation of Cajal-Retzius subtypes. *J Neurosci*. 27:11103–11111.

Hanashima C, Li SC, Shen L, Lai E, Fishell G. 2004. Foxg1 suppresses early cortical cell fate. *Science*. 303:56–59.

Hanashima C, Shen L, Li SC, Lai E. 2002. Brain factor-1 controls the proliferation and differentiation of neocortical progenitor cells through independent mechanisms. *J Neurosci*. 22:6526–6536.

He X-B, Yi S-H, Rhee Y-H, Kim H, Han Y-M, Lee S-H, Lee H, Park C-H, Lee Y-S, Richardson E *et al*. 2011. Prolonged membrane depolarization enhances midbrain dopamine neuron differentiation via epigenetic histone modifications. *Stem Cells*. 29:1861–1873.

Hong EJ, McCord AE, Greenberg ME. 2008. A biological function for the neuronal activity-dependent component of Bdnf transcription in the development of cortical inhibition. *Neuron*. 60:610–624.

Hou P-S, Miyoshi G, Hanashima C. 2019. Sensory cortex wiring requires preselection of short- and long-range projection neurons through an Egr-Foxg1-COUP-TFI network. *Nat Commun*. 10:3581.

Jancic D, Lopez de Armentia M, Valor LM, Olivares R, Barco A. 2009. Inhibition of cAMP response element-binding protein reduces neuronal excitability and plasticity, and triggers neurodegeneration. *Cereb Cortex*. 19:2535–2547.

Jembrek M, Vlainic J. 2015. GABA receptors: pharmacological potential and pitfalls. *Curr Pharm Des*. 21:4943–4959.

Johnston J, Forsythe ID, Kopp-Scheinpflug C. 2010. SYMPOSIUM REVIEW: going native: voltage-gated potassium channels controlling neuronal excitability: K^+ channels and auditory processing. *J Physiol*. 588:3187–3200.

Jones MW, Errington ML, French PJ, Fine A, Bliss TV, Garel S, Charnay P, Bozon B, Laroche S, Davis S. 2001. A requirement for the immediate early gene Zif268 in the expression of late LTP and long-term memories. *Nat Neurosci*. 4:289–296.

Kawashima T, Okuno H, Nonaka M, Adachi-Morishima A, Kyo N, Okamura M, Takemoto-Kimura S, Worley PF, Bito H. 2009. Synaptic activity-responsive element in the arc/Arg3.1 promoter essential for synapse-to-nucleus signaling in activated neurons. *Proc Natl Acad Sci U S A*. 106:316–321.

Koldamova R, Schug J, Lefterova M, Cronican AA, Fitz NF, Davenport FA, Carter A, Castranio EL, Lefterov I. 2014. Genome-wide approaches reveal EGR1-controlled regulatory networks associated with neurodegeneration. *Neurobiol Dis*. 63:107–114.

Kim T-K, Hemberg M, Gray JM, Costa AM, Bear DM, Wu J, Harmin DA, Laptewicz M, Barbara-Haley K, Kuersten S *et al*. 2010. Widespread transcription at neuronal activity-regulated enhancers. *Nature*. 465:182–187.

Kwon S-K, Hirabayashi Y, Polleux F. 2016. Organelle-specific sensors for monitoring Ca^{2+} dynamics in neurons. *Front Synaptic Neurosci*. 8:29.

Lopez de Armentia M, Jancic D, Olivares R, Alarcon JM, Kandel ER, Barco A. 2007. cAMP response element-binding protein-mediated gene expression increases the intrinsic excitability of CA1 pyramidal neurons. *J Neurosci*. 27: 13909–13918.

Manuel M, Martynoga B, Yu T, West JD, Mason JO, Price DJ. 2010. The transcription factor Foxg1 regulates the competence of telencephalic cells to adopt subpallial fates in mice. *Development*. 137:487–497.

Mariani J, Coppola G, Zhang P, Abyzov A, Provini L, Tomasini L, Amenduni M, Szekely A, Palejev D, Wilson M *et al*. 2015. FOXG1-dependent dysregulation of GABA/glutamate neuron differentiation in autism spectrum disorders. *Cell*. 162:375–390.

Martynoga B, Morrison H, Price DJ, Mason JO. 2005. Foxg1 is required for specification of ventral telencephalon and region-specific regulation of dorsal telencephalic precursor proliferation and apoptosis. *Dev Biol*. 283:113–127.

Mathelier A, Zhao X, Zhang AW, Parcy F, Worsley-Hunt R, Arenillas DJ, Buchman S, Chen C, Chou A, Ienasescu H *et al*. 2014. JASPAR 2014: an extensively expanded and updated open-access database of transcription factor binding profiles. *Nucleic Acids Res*. 42:D142–D147.

Mayer SI, Dexheimer V, Nishida E, Kitajima S, Thiel G. 2008. Expression of the transcriptional repressor ATF3 in gonadotrophs is regulated by Egr-1, CREB, and ATF2 after gonadotropin-releasing hormone receptor stimulation. *Endocrinology*. 149:6311–6325.

Mitter D, Pringsheim M, Kaulisch M, Plümacher KS, Schröder S, Warthemann R, Abou Jamra R, Baethmann M, Bast T *et al*. 2018. FOXG1 syndrome: genotype–phenotype association in 83 patients with FOXG1 variants. *Genet Med*. 20:98–108.

Miyoshi G, Fishell G. 2012. Dynamic FoxG1 expression coordinates the integration of multipolar pyramidal neuron precursors into the cortical plate. *Neuron*. 74:1045–1058.

Molyneaux BJ, Arlotta P, Menezes JRL, Macklis JD. 2007. Neuronal subtype specification in the cerebral cortex. *Nat Rev Neurosci*. 8:427–437.

Monteiro P, Feng G. 2017. SHANK proteins: roles at the synapse and in autism spectrum disorder. *Nat Rev Neurosci*. 18:147–157.

Muzio L, Mallamaci A. 2005. Foxg1 confines Cajal-Retzius neuronogenesis and hippocampal morphogenesis to the dorsomedial pallium. *J Neurosci*. 25:4435–4441.

Olive M, Krylov D, Echlin DR, Gardner K, Taparowsky E, Vinson C. 1997. A dominant negative to activation protein-1 (AP1) that abolishes DNA binding and inhibits oncogenesis. *J Biol Chem*. 272:18586–18594.

Paoletti P, Bellone C, Zhou Q. 2013. NMDA receptor subunit diversity: impact on receptor properties, synaptic plasticity and disease. *Nat Rev Neurosci*. 14:383–400.

Park EA, Song S, Vinson C, Roesler WJ. 1999. Role of CCAAT enhancer-binding protein beta in the thyroid hormone and cAMP induction of phosphoenolpyruvate carboxykinase gene transcription. *J Biol Chem*. 274:211–217.

Paternain AV, Cohen A, Stern-Bach Y, Lerma J. 2003. A role for extracellular Na+ in the channel gating of native and recombinant kainate receptors. *J Neurosci*. 23:8641–8648.

Patriarchi T, Amabile S, Frullanti E, Landucci E, Lo Rizzo C, Ariani F, Costa M, Olimpico F, W Hell J, M Vaccarino F *et al*. 2016. Imbalance of excitatory/inhibitory synaptic protein expression in iPSC-derived neurons from *FOXG1*$^{+/-}$ patients and in *Foxg1*$^{+/-}$ mice. *Eur J Hum Genet*. 24:871–880.

Penke Z, Morice E, Veyrac A, Gros A, Chagneau C, LeBlanc P, Samson N, Baumgartel K, Mansuy IM, Davis S *et al*. 2013. Zif268/Egr1 gain of function facilitates hippocampal synaptic plasticity and long-term spatial recognition memory. *Philos Trans R Soc B Biol Sci*. 369:20130159–20130159.

Pikaart MJ, Recillas-Targa F, Felsenfeld G. 1998. Loss of transcriptional activity of a transgene is accompanied by DNA methylation and histone deacetylation and is prevented by insulators. *Genes Dev*. 12:2852–2862.

Racine RJ. 1972. Modification of seizure activity by electrical stimulation. II. Motor seizure. *Electroencephalogr Clin Neurophysiol*. 32:281–294.

Raffaello A, Mammucari C, Gherardi G, Rizzuto R. 2016. Calcium at the center of cell signaling: interplay between endoplasmic reticulum, mitochondria, and lysosomes. *Trends Biochem Sci*. 41:1035–1049.

Raponi E, Agenes F, Delphin C, Assard N, Baudier J, Legraverend C, Deloulme J-C. 2007. S100B expression defines a state in which GFAP-expressing cells lose their neural stem cell potential and acquire a more mature developmental stage. *Glia*. 55:165–177.

Rauti R, Lozano N, León V, Scaini D, Musto M, Rago I, Ulloa Severino FP, Fabbro A, Casalis L, Vázquez E *et al*. 2016. Graphene oxide nanosheets reshape synaptic function in cultured brain networks. *ACS Nano*. 10:4459–4471.

Rivera C, Voipio J, Payne JA, Ruusuvuori E, Lahtinen H, Lamsa K, Pirvola U, Saarma M, Kaila K. 1999. The K^+/Cl^- co-transporter KCC2 renders GABA hyperpolarizing during neuronal maturation. *Nature*. 397:251–255.

Ryan TJ, Roy DS, Pignatelli M, Arons A, Tonegawa S. 2015. Engram cells retain memory under retrograde amnesia. *Science*. 348:1007–1013.

Sanchez RM, Koh S, Rio C, Wang C, Lamperti ED, Sharma D, Corfas G, Jensen FE. 2001. Decreased glutamate receptor 2 expression and enhanced epileptogenesis in immature rat hippocampus after perinatal hypoxia-induced seizures. *J Neurosci*. 21:8154–8163.

Sanganahalli BG, Herman P, Hyder F, Kannurpatti SS. 2013. Mitochondrial calcium uptake capacity modulates neocortical excitability. *J Cereb Blood Flow Metab*. 33:1115–1126.

Schwarz EM, Van Antwerp D, Verma IM. 1996. Constitutive phosphorylation of IkappaBalpha by casein kinase II occurs preferentially at serine 293: requirement for degradation of free IkappaBalpha. *Mol Cell Biol*. 16:3554–3559.

Seltzer LE, Ma M, Ahmed S, Bertrand M, Dobyns WB, Wheless J, Paciorkowski AR. 2014. Epilepsy and outcome in FOXG1-related disorders. *Epilepsia*. 55:1292–1300.

Seuntjens E, Nityanandam A, Miquelajauregui A, Debruyn J, Stryjewska A, Goebbels S, Nave K-A, Huylebroeck D, Tarabykin V. 2009. Sip1 regulates sequential fate decisions by feedback signaling from postmitotic neurons to progenitors. *Nat Neurosci*. 12:1373–1380.

Shah NH, Aizenman E. 2014. Voltage-gated potassium channels at the crossroads of neuronal function, ischemic tolerance, and neurodegeneration. *Transl Stroke Res*. 5:38–58.

Shen W, Ba R, Su Y, Ni Y, Chen D, Xie W, Pleasure SJ, Zhao C. 2019. Foxg1 regulates the postnatal development of cortical interneurons. *Cereb Cortex*. 29(4):1547–1560.

Snow WM, Albensi BC. 2016. Neuronal gene targets of NF-κB and their dysregulation in Alzheimer's disease. *Front Mol Neurosci*. 9:118.

Striano P, Paravidino R, Sicca F, Chiurazzi P, Gimelli S, Coppola A, Robbiano A, Traverso M, Pintaudi M, Giovannini S *et al*.

2011. West syndrome associated with 14q12 duplications harboring FOXG1. *Neurology*. 76:1600–1602.

Sun Y, Paşca SP, Portmann T, Goold C, Worringer KA, Guan W, Chan KC, Gai H, Vogt D, Chen Y-JJ *et al*. 2016. A deleterious Nav1.1 mutation selectively impairs telencephalic inhibitory neurons derived from Dravet syndrome patients. *elife*. 5:e13073.

Tamamaki N, Yanagawa Y, Tomioka R, Miyazaki J-I, Obata K, Kaneko T. 2003. Green fluorescent protein expression and colocalization with calretinin, parvalbumin, and somatostatin in the GAD67-GFP knock-in mouse. *J Comp Neurol*. 467:60–79.

Toma K, Kumamoto T, Hanashima C. 2014. The timing of upper-layer neurogenesis is conferred by sequential derepression and negative feedback from deep-layer neurons. *J Neurosci*. 34:13259–13276.

Traynelis SF, Wollmuth LP, McBain CJ, Menniti FS, Vance KM, Ogden KK, Hansen KB, Yuan H, Myers SJ, Dingledine R. 2010. Glutamate receptor ion channels: structure, regulation, and function. *Pharmacol Rev*. 62:405–496.

Tyssowski KM, DeStefino NR, Cho J-H, Dunn CJ, Poston RG, Carty CE, Jones RD, Chang SM, Romeo P, Wurzelmann MK *et al*. 2018. Different neuronal activity patterns induce different gene expression programs. *Neuron*. 98(3):530–546.e11.

Van Antwerp DJ, Martin SJ, Kafri T, Green DR, Verma IM. 1996. Suppression of TNF-alpha-induced apoptosis by NF-kappaB. *Science*. 274:787–789.

Vegas N, Cavallin M, Maillard C, Boddaert N, Toulouse J, Schaefer E, Lerman-Sagie T, Lev D, Magalie B, Moutton S *et al*. 2018. Delineating FOXG1 syndrome: from congenital microcephaly to hyperkinetic encephalopathy. *Neurol Genet*. 4:e281.

Viosca J, Lopez de Armentia M, Jancic D, Barco A. 2009. Enhanced CREB-dependent gene expression increases the excitability of neurons in the basal amygdala and primes the consolidation of contextual and cued fear memory. *Learn Mem*. 16:193–197.

Wada A, Takahashi H, Lipton SA, Chen H-SV. 2006. NR3A modulates the outer vestibule of the "NMDA" receptor channel. *J Neurosci*. 26:13156–13166.

Wamsley B, Fishell G. 2017. Genetic and activity-dependent mechanisms underlying interneuron diversity. *Nat Rev Neurosci*. 18:299–309.

Wisden W, Seeburg PH. 1993. A complex mosaic of high-affinity kainate receptors in rat brain. *J Neurosci*. 13:3582–3598.

Yassin L, Benedetti BL, Jouhanneau J-S, Wen JA, Poulet JFA, Barth AL. 2010. An embedded subnetwork of highly active neurons in the neocortex. *Neuron*. 68:1043–1050.

Zamponi GW, Lory P, Perez-Reyes E. 2010. Role of voltage-gated calcium channels in epilepsy. *Pflugers Arch - Eur J Physiol*. 460:395–403.

Zhou Y, Won J, Karlsson MG, Zhou M, Rogerson T, Balaji J, Neve R, Poirazi P, Silva AJ. 2009. CREB regulates excitability and the allocation of memory to subsets of neurons in the amygdala. *Nat Neurosci*. 12:1438–1443.

Zhu W, Zhang B, Li M, Mo F, Mi T, Wu Y, Teng Z, Zhou Q, Li W, Hu B. 2019. Precisely controlling endogenous protein dosage in hPSCs and derivatives to model FOXG1 syndrome. *Nat Commun*. 10(1):928.